Free Vibration Analysis of HVAC Ducts

Chavan Pruthviraj Namdeo

ME10M01

A Dissertation Submitted to

Indian Institute of Technology Hyderabad

In Partial Fulfillment of the Requirements for

The Degree of Master of Technology

भारतीय प्रौद्योगिकी संस्थान हैदराबाद

Indian Institute of Technology Hyderabad

Department of Mechanical Engineering

June, 2012

Declaration

I declare that this written submission represents my ideas in my own words, and where others' ideas or words have been included, I have adequately cited and referenced the original sources. I also declare that I have adhered to all principles of academic honesty and integrity and have not misrepresented or fabricated or falsified any idea/data/fact/source in my submission. I understand that any violation of the above will be a cause for disciplinary action by the Institute and can also evoke penal action from the sources that have thus not been properly cited, or from whom proper permission has not been taken when needed.

<div align="right">

Rhavan

(Signature)

Chavan Pruthviraj Namdeo

(ME10M01)

</div>

Approval Sheet

This thesis entitled "Free Vibration Analysis of HVAC Ducts" by Chavan Pruthviraj Namdeo is approved for the degree of Master of Technology from IIT Hyderabad.

Dr. R. Prasanth Kumar

Assistant Professor IITH

Examiner

4 July 2012

Dr. Chandrika Prakash Vyasarayani

Assistant Professor IITH

Examiner

Dr. B. Venkatesham

Assistant Professor IITH

Adviser

Dr. B. Umashankar

Assistant Professor IITH

Chairman

Acknowledgements

Dedicated to

My lovely Dada and Aai

Abstract

Free vibration analysis of ducts is the first step to understand the coupling between structural and acoustic modes in Heating, Ventilation and Air Conditioning (HVAC) ducts. This thesis covers free vibration analysis of different duct shapes like rectangular, circular, flat oval and elliptical. These types of ducts are extensively used in HVAC systems. Transfer Matrix (TM) method is used to calculate natural frequencies and mode shapes for rectangular and flat oval ducts with simply supported boundary conditions. Free vibration analysis of cylindrical ducts and curved plates is explained as subsections of flat oval ducts. TM method is only useful for simply supported boundary conditions.

Rayleigh-Ritz method with static beam solutions as admissible functions is used for analysis of rectangular ducts with different axial boundary conditions. Analytical model results are corroborated with Finite Element (FEM) results and also with available literature data for respective ducts. Validated Rayleigh-Ritz method is used for parametric studies of rectangular ducts and to generate tabular engineering data of non-dimensional frequency parameter for different combinations of aspect ratios and side ratios of rectangular ducts. A simple empirical relation is presented, which can predict the first fundamental frequency for any dimension of rectangular duct with different boundary conditions and different material properties.

Elliptical duct modal parameters are measured using Experimental Modal Analysis (EMA). FEM results of elliptical duct are used as guidelines to set up the procedure. EMA of cantilever beam has been done as a test case. Modal validation has been done between FEM data and EMA data by calculating Modal Assurance Criteria (MAC) numbers for respective modes.

Nomenclature

X, Y, Z	Cartesian coordinate system
X, S, Z	Cylindrical coordinate system
u, v, w	Deflections in X, Y, Z directions respectively
M_x, M_s, M_{sx}	Moments in X, S directions
N_x, N_s, N_{sx}	Components of membrane force
L_1, L_2	Cross – section dimensions of rectangular duct
H	Non – dimensional cross section parameter
ψ	Slope
S_s	Kelvin – Kirchhoff shearing force
E, ρ, μ	Young's modulus, density and poisons ratio of material respectively
λ	Frequency parameter
f	Natural frequency in Hz
$[\mathbf{A}]$	State space matrix
L_r, h_r	Length and thickness of rectangular duct
R_{cp}, L_{cp}, h_{cp}	Radius, length and thickness of curved plate
R_{cd}, L_{cd}, h_{cd}	Radius, length and thickness of circular duct
R_f, B_f	Cross section dimension of flat oval duct
L_f, h_f	Length and thickness of flat oval duct
L_t , L_{fc}	Total cross – section length of rectangular and flat oval duct respectively
S_1, S_2	Side and aspect ratios respectively for rectangular duct
m , n	Axial and circumferential half wave number
$\mathbf{P}$	Point matrix
D, K	Extensional and flexural rigidities
ξ	Angle between flat plate and curved plate of flat oval duct
θ	Angle described by curved plate
E_1, E_2	Major and minor axis of elliptical duct
MCA_{ij}	MAC number between ith EMA and jth FEM mode

List of Figures

List of Tables

Contents

Chapter 1

Introduction

1.1 Motivation

Heating, Ventilation and Air-conditioning (HVAC) systems extensively uses ducts of different size and shapes connected in series or parallel. Most prominent duct shapes are rectangular, circular, flat oval and elliptical. These ducts are mostly used for the air handling purpose in these HVAC systems. Noise generated from the HVAC systems propagate in axial and transverse directions of a duct. While propagating some amount of noise tends to radiate in transverse direction. Noise radiated from duct in the transverse direction is called as breakout noise. This breakout noise from these ducts is of research interest and research papers can be seen in this direction. B. Venkatesham et al. [1, 2] discussed prediction of breakout noise from a rectangular duct with compliant walls and from an elliptical duct of finite length. The coupling of acoustic duct modes and structural duct modes plays a critical role in generating noise in transverse direction. It is important to understand this coupling to know the breakout noise thorough ducts. The first step in understanding of the structural-acoustic coupling is to know the modal characteristics of these ducts (i.e. Natural frequencies, mode shapes and damping).

Figure 1 shows schematic diagrams of different type of duct, used in HVAC systems.
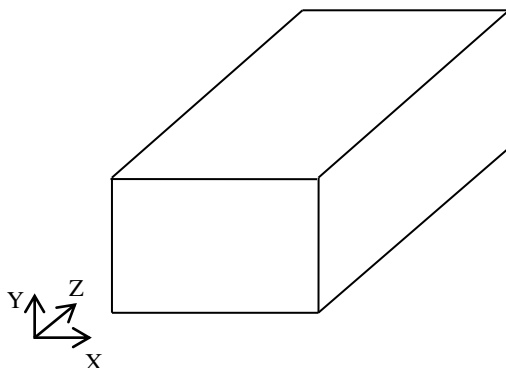
Figure 1 (a) : Rectangular duct
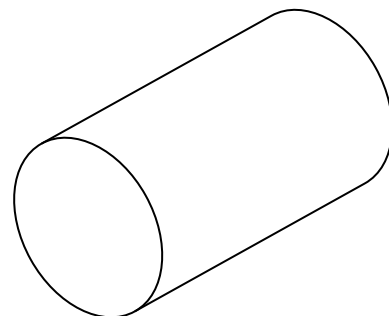
Figure 1 (b) Circular duct
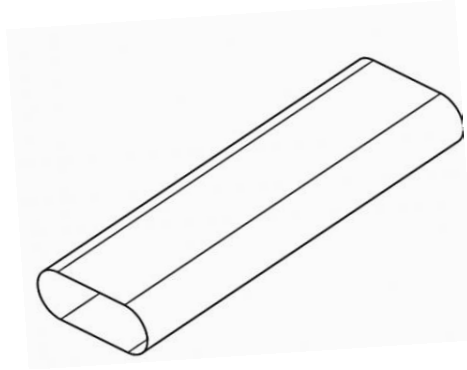
Figure 1 (c): Flat Oval Duct

1.2 Literature survey

Rectangular duct has highest breakout noise compared to circular and flat oval duct cross-section due to lower stiffness of these ducts. High noise radiation in transverse direction occurs at a coupling frequency between acoustic subsystem (duct-interior space) and structural subsystem (duct walls). The calculation of coupling frequency depends on two subsystems natural frequencies. So, developing a simple analytical model to calculate natural frequencies of different ducts, with different boundary conditions is of research interest. Literature suggests that different methods are available for free vibration analysis of rectangular duct. Broadly these methods are classified into four categories (1) Transfer Matrix method (2) Receptance method (3) Rayleigh-Ritz method (4) Finite Element method. Every method has its own advantages and limitations.

S. Azimi et al. [3], G. Yamada et al. [4] used the receptance method. H. P. Lee [5] used Rayleigh-Ritz method for calculating the natural frequencies and mode shape of polygonal ducts. T. Irea, et al. [6] used transfer matrix method for free vibration analysis of prismatic shells. Sai Jagan Mohan, et al. [7] used Finite Element Method to calculate natural frequencies and mode shape. They used group theoretical analysis to characterize duct modes. In the present thesis the free vibration analysis of rectangular duct is explained by using the transfer matrix method for simple–simple supported axial boundary conditions and Rayleigh-Ritz method for different axial boundary conditions. The transfer matrix method is very much suitable for the vibration analysis of structures whose mass and stiffness components can be considered as distributed along the line. Advantage of transfer matrix over other methods is that, it is very easy to implement with the simply supported boundary conditions. In the transfer matrix analysis of a rectangular duct, only quarter section of the duct is considered with symmetrical boundary conditions at the ends. This configuration is equivalent to folded plate with an angle of 90^0 between them. Research can be seen in the transfer matrix analysis and free vibration of folded plates. T. Irie, et al. [8–11] used the transfer matrix method for the natural frequency analysis of folded plate, analysis of non-circular cylindrical shells with longitudinal interior partitions, analysis of joining conical–cylindrical shells and of the conical shell with variable thickness.

Existing literature has been considered only simply supported boundary conditions in axial direction of the duct. According to the authors, there is no work reported for other axial boundary conditions. Transfer matrix analysis mostly considers only simply supported boundary conditions in the axial direction. One more method is proposed i.e. Rayleigh-Ritz method with static beam functions as admissible functions to account for different boundary conditions. A good amount of literature is available for the Rayleigh-Ritz methods with different admissible functions. Selection of the proper admissible function provides variation in Rayleigh-Ritz method. Admissible function varies based on application like rectangular plate, rectangular plate with intermediate supports etc. Zhou Ding [12] used the Rayleigh-Ritz method for natural frequency analysis of rectangular plates with a set of static beam function as admissible function. D. Zhou et al. [13] used a set of static beam functions for free vibration analysis of rectangular plates with intermediate supports. In the present paper, rectangular duct modeled as an unfolded plate with rotational springs at ends and edges modeled as intermediate support. The set of static beam functions are extended for the rectangular ducts. In Rayleigh-Ritz method, validity and accuracies are entirely depends upon the choice of the admissible functions. These static beam functions are the static solutions of the point supported beam under sine loads.

Calculated results from these methods for rectangular duct validated with the available literature data and with finite element method (FEM) results. Parametric study for different sizes of rectangular ducts with different material properties is also reported. The validated analytical model is used to generate the engineering data for the rectangular ducts with different side ratios (height to width or width to height of the duct) and with different aspect ratios (perimeter of the duct cross section to length of the duct). These ratios are taken as four step values (0.25, 0.5, 0.75, 1). Further curve fitting has been done for generating engineering data results and an empirical relation has been developed to calculate the first fundamental frequency. Mode shapes of rectangular duct are classified into four groups. This classification is done similar to the classification made by the Tian Ran et al. [14] for box-type structure.

Moreover the transfer matrix method is also used for analysis of flat oval ducts and cylindrical ducts. Minimal literature has been reported for free vibration analysis of flat oval duct but there is a good amount of research articles are available related to vibration analysis of cylindrical ducts. Basen Alzahabi and Logesh Kumar Natrajan [15] used experimental modal analysis for analysis of simply supported cylindrical ducts. Gamma Xie [16] used transfer matrix method with Flugge shell theory to explain the free vibration analysis of cylindrical ducts. In the present analysis of flat oval ducts and cylindrical ducts, the transfer matrix method is used with Goldenveizer-Novozhilov shell theory. M. Ohga et al. [17] explained natural frequencies and mode shapes of open cylindrical shells with a circumferential taper by using transfer matrix with Goldenveizer-Novozhilov shell theory. For transfer matrix analysis only, quarter section of flat oval duct and cylindrical ducts are considered with symmetrical boundary conditions at the ends. A quarter section of flat oval duct

consists of one curved plate and one flat plate. As the analysis started with the shell theory, first transfer matrix method is defined for the curved plates then for cylindrical ducts and finally for flat oval ducts. Results from the transfer matrix method are compared with FEM results, for validation.

Experimental Modal Analysis (EMA) is used for analyzing elliptical duct. EMA is the classical way of finding out modal characteristics of the structures. EMA is most widely used for this purpose even from simple structures like beams to very complicated structures like Aircraft wings, Automobile body etc. In the present work, EMA is used for modal analysis of cantilever beam and for elliptical duct with free – free boundary conditions. EMA study of cantilever beam helped us to understand the procedure. The elliptical duct problem is handled by using two techniques, Single Degree Freedom (SDOF) system and Multi Degree Freedom (MDOF) system. Before setting up actual experiment, FEM analysis has been done for respective structure. This helps in deciding the frequency range of interest, accelerometer position, impact hammer requirement and measurement points. In EMA, initially time domain data have been collected by providing excitation at some locations with impact hammer. Vibration response has been measured by using accelerometer at one location. This actually called as a roving hammer technique in which position of accelerometer is fixed and a hammer is used to excite structure at different points. The measured time domain data converted to frequency domain data to get the frequency response function (FRF). Peaks of FRF data relates to the Natural frequencies of the structure. Mode shapes are obtained by analyzing the deflection pattern at the particular peak in FRF. For EMA, some assumptions have been made i.e. material is homogeneous and boundary conditions are perfectly clamped or free-free. Modal Assurance Criteria (MAC) has been calculated between experimental data and FEM data using a commercial package (LMS Virtual Lab).

FEM analysis has been done using a commercial package (ANSYS 13). Modeling details about boundary conditions and meshing details are discussed in chapter number five.

Chapter 2

Rectangular Duct

Free vibration analysis of rectangular ducts is studied by using two methods, transfer matrix method for simplicity-simple supported boundary conditions and Rayleigh-Ritz method for different axial boundary conditions.

2.1   Transfer Matrix method

Transfer matrix method relates upstream and downstream state space variables in a matrix form called as transfer matrix. At first a simple matrix is formulated from free vibration governing equations. This matrix is similar to the state space representation. Solution for governing equation is arranged in a matrix form to get the transfer matrix, in which only frequency parameter is unknown. Then this problem is solved similar to eigenvalue problem. Eigen solutions to frequency parameter are nothing but natural frequencies for the duct and eigen vector gives the mode shapes for respective frequencies.

For transfer matrix analysis only quarter section of ducts are considered with symmetric boundary conditions at the ends. Figure 2 (a) shows a schematic diagram of a cross section of a rectangular duct. The duct cross-section is geometrically symmetric about X and Y axis. The quarter section is shown in Fig. 2 (b).
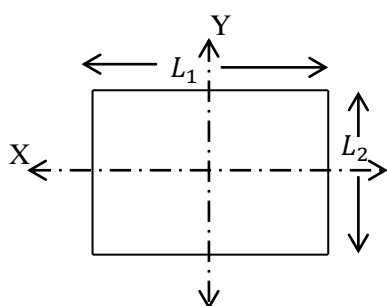
Figure 2(a): Rectangular duct cross section   **Figure 2(b): Quarter section of the duct**
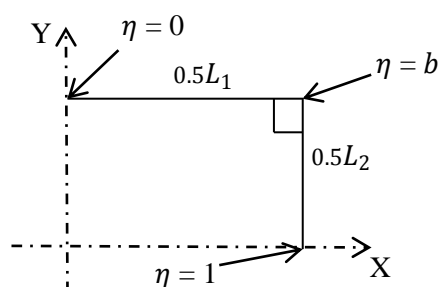
A quarter section of the duct can be modeled as a folded plate with angle of 90^0. T. Irie, et al. [8] discussed calculations of the natural frequencies for folded plate with free edge boundary

conditions in circumferential directions. To define total transfer matrix for a quarter section of rectangular duct shown in Figure 2 (b), requires one transfer matrix to relate the state space variables at $\eta = 0$ to $\eta = b$, point matrix to relate variables across the joint and one more transfer matrix to relate the variable from $\eta = b$ to $\eta = 1$. Condition at folding joint can be expressed as a point matrix. It gives the relationship between state vectors at the joint.

As the quarter section considered as folded plate with 90^0 angle between them. First Goldenveizer-Novozhilov free vibration equations of shells with simply supported boundary conditions are arranged in a matrix differential form. This matrix is modified for the plates. State space matrix in differential form is given as,

$$
d/ds \begin{Bmatrix} \bar{u} \\ \bar{v} \\ \bar{w} \\ \bar{\psi} \\ \overline{M_s} \\ -\overline{S_s} \\ \overline{N_s} \\ -\overline{N_{sx}} \end{Bmatrix} = \begin{bmatrix} 0 & A_{12} & 0 & 0 & 0 & 0 & 0 & A_{18} \\ A_{21} & 0 & 0 & 0 & 0 & 0 & A_{27} & \\ 0 & 0 & 0 & A_{34} & 0 & 0 & & \\ 0 & 0 & A_{43} & 0 & A_{45} & & & \\ A & 0 & 0 & A_{54} & & & & \\ 0 & 0 & A_{63} & & & SYM & & \\ 0 & A_{72} & & & & & & \\ A_{81} & & & & & & & \end{bmatrix} \begin{Bmatrix} \bar{u} \\ \bar{v} \\ \bar{w} \\ \bar{\psi} \\ \overline{M_s} \\ -\overline{S_s} \\ \overline{N_s} \\ -\overline{N_{sx}} \end{Bmatrix} \qquad (1)
$$

Components of this matrix are given in appendix.

The above equation can also be written as,

$$
\left(\frac{d}{d\eta} \right) Z(\eta) = [\mathbf{A}] * Z(\eta) \qquad (2)
$$

$Z(\eta)$ is state vector which can also be expressed as,

$$
Z(\eta)|_{\eta_1} = \mathbf{T}(\mathbf{\eta}, \mathbf{\eta_0}) * Z(\eta_0)|_{\eta_0} \qquad (3)
$$

Where,

$\mathbf{T}(\mathbf{\eta}, \mathbf{\eta_0})$ represents the Transfer Matrix which relates space vectors at η_0 to η_1. Elements of this transfer matrix are calculated by using Runge-Kutta-Gill integration method. So the total transfer matrix to relate the space variable of a quarter section of rectangular duct (shown in fig. 2 (b)) can be written as,

$$
Z(\eta)|_\eta = \begin{cases} \mathbf{T}(\mathbf{b}, \mathbf{\eta_0}) Z(\eta)|_{\eta=0} & (\eta < b) \\ \mathbf{T}(\mathbf{\eta_1}, \mathbf{b}) \mathbf{P} \mathbf{T}(\mathbf{b}, \mathbf{\eta_0}) Z(\eta)|_{\eta=0} & (\eta > b) \end{cases} \qquad (4)
$$

Where,

$\mathbf{T}(\mathbf{b}, \mathbf{\eta_0})$ is the transfer matrix for first flat plate from $\eta = 0$ to b point, $\mathbf{T}(\mathbf{\eta_1}, \mathbf{b})$ is the transfer matrix for the second flat plate i.e from b point to $\eta = 1$ and $\mathbf{P}$ is point matrix which is defined as,

$$\mathbf{P} = \begin{bmatrix} 1 & 0 & 0 & 0 & 0 & 0 & 0 & 0 \\ 0 & 0 & -1 & 0 & 0 & 0 & 0 & 0 \\ 0 & 1 & 0 & 0 & 0 & 0 & 0 & 0 \\ 0 & 0 & 0 & 1 & 0 & 0 & 0 & 0 \\ 0 & 0 & 0 & 0 & 1 & 0 & 0 & 0 \\ 0 & 0 & 0 & 0 & 0 & 0 & -1 & 0 \\ 0 & 0 & 0 & 0 & 0 & 1 & 0 & 0 \\ 0 & 0 & 0 & 0 & 0 & 0 & 0 & 1 \end{bmatrix} \tag{5}$$

Total transfer matrix is of (8×8) in size and it has eight state space variables, which can be written as,

$$\left\{ \begin{array}{c} \bar{u} \\ \bar{v} \\ \bar{w} \\ \bar{\psi} \\ \overline{M_s} \\ -\overline{S_s} \\ \overline{N_s} \\ -\overline{N_{sx}} \end{array} \right\}_\eta = \begin{bmatrix} T_{11} & T_{12} & T_{13} & T_{14} & T_{15} & T_{16} & T_{17} & T_{18} \\ T_{21} & T_{22} & T_{23} & T_{24} & T_{25} & T_{26} & T_{27} & T_{28} \\ T_{31} & T_{32} & T_{33} & T_{34} & ... & ... & ... & \vdots \\ \vdots & \vdots & \vdots & \vdots & \vdots & \vdots & \vdots & \vdots \\ \vdots & \vdots & \vdots & \vdots & \vdots & \vdots & \vdots & \vdots \\ \vdots & \vdots & \vdots & \vdots & \vdots & \vdots & \vdots & \vdots \\ \vdots & \vdots & \vdots & \vdots & \vdots & \vdots & \vdots & \vdots \\ T_{81} & ... & ... & ... & ... & ... & ... & T_{88} \end{bmatrix} \left\{ \begin{array}{c} \bar{u} \\ \bar{v} \\ \bar{w} \\ \bar{\psi} \\ \overline{M_s} \\ -\overline{S_s} \\ \overline{N_s} \\ -\overline{N_{sx}} \end{array} \right\}_{\eta_0} \tag{6}$$

Symmetrical boundary conditions at symmetrical plane written as,

$v = \psi = S_s = N_{sx} = 0$ for Symmetric(S) mode (7a)

$u = w = M_s = N_s = 0$ for anti-symmetric (AS) mode. (7b)

By applying these boundary conditions, four types of vibration modes can be observed in the duct. These modes are symmetric or anti-symmetric with respect to two symmetric planes.

These modes are S-S, S-AS, AS-S, AS-AS. By substituting the symmetry plane boundary conditions for different modes this 8×8 matrix will be reduced to 4×4 matrix. By solving these matrices as eigenvalue problem, gives the natural frequencies and associated mode shapes. The symmetry plane boundary conditions for each mode and the matrix obtained is given below.

S-S mode:

At $\eta=\eta_0$, $\quad v = \psi = S_s = N_{sx} = 0$ $\quad$ and (8a)
at $\eta=1$, $\quad v = \psi = S_s = N_{sx} = 0$. (8b)

Substituting equation (8) in to the equation (6) leads all even columns can be avoided. Similarly, the second boundary condition leads to all even row values need to be considered.

The final frequency matrix can be written as below

$$\begin{bmatrix} T_{21} & T_{23} & T_{25} & T_{27} \\ T_{41} & T_{43} & T_{45} & T_{47} \\ T_{61} & T_{63} & T_{65} & T_{67} \\ T_{81} & T_{83} & T_{85} & T_{87} \end{bmatrix} \begin{bmatrix} u \\ w \\ M_s \\ N_s \end{bmatrix}_{\eta=\eta_0} = 0 \tag{9}$$

AS-S mode :

at $\eta=\eta_0$, $\quad u = w = M_s = N_s = 0$ $\quad$ and (10a)
at $\eta=1$, $\quad v = \psi = S_s = N_{sx} = 0$. (10b)

First boundary condition leads to all odd column values are avoided. Second boundary condition leads to all even row values need to be considered.

The final frequency matrix can be written as,

$$
\begin{bmatrix}
T_{22} & T_{24} & T_{26} & T_{28} \\
T_{42} & T_{44} & T_{46} & T_{48} \\
T_{62} & T_{64} & T_{66} & T_{68} \\
T_{82} & T_{84} & T_{86} & T_{88}
\end{bmatrix}
\begin{bmatrix}
v \\
\psi \\
-S_s \\
-N_{sx}
\end{bmatrix}_{\eta=\eta_0} = 0
\tag{11}
$$

S-AS mode:

at $\eta=\eta_0$, $v = \psi = S_s = N_{sx} = 0$ and $\qquad\qquad\qquad\qquad\qquad$ (12a)
at $\eta=1$, $u = w = M_s = N_s = 0$ $\qquad\qquad\qquad\qquad\qquad\qquad\quad$ (12b)

The final frequency matrix can be written as,

$$
\begin{bmatrix}
T_{11} & T_{13} & T_{15} & T_{17} \\
T_{31} & T_{33} & T_{35} & T_{37} \\
T_{51} & T_{53} & T_{55} & T_{57} \\
T_{71} & T_{73} & T_{75} & T_{77}
\end{bmatrix}
\begin{bmatrix}
u \\
w \\
M_s \\
N_s
\end{bmatrix}_{\eta=\eta_0} = 0
\tag{13}
$$

AS-AS mode:

at $\eta=\eta_0$, $u = w = M_s = N_s = 0$ and $\qquad\qquad\qquad\qquad\qquad$ (14a)
at $\eta=1$, $u = w = M_s = N_s = 0$ $\qquad\qquad\qquad\qquad\qquad\qquad\quad$ (14b)

The final frequency matrix can be written as,

$$
\begin{bmatrix}
T_{12} & T_{14} & T_{16} & T_{18} \\
T_{32} & T_{34} & T_{36} & T_{38} \\
T_{52} & T_{54} & T_{56} & T_{58} \\
T_{72} & T_{74} & T_{76} & T_{78}
\end{bmatrix}
\begin{bmatrix}
v \\
\psi \\
-S_s \\
-N_{xs}
\end{bmatrix}_{\eta=\eta_0} = 0
\tag{15}
$$

The frequency parameter λ is unknown which can be determined by calculating eigenvalues of these matrices. The natural frequencies are obtained by the following equation,

$$
f = [\lambda/2\pi L_t]\sqrt{E/\rho(1 - \mu^2)}
\tag{16}
$$

Where,

$$
L_t = 0.5(L_1 + L_2)
$$

Mode shapes can be obtained by back substituting the values of λ in the equations 9, 11, 13 and 15 for the respective modes.

8

2.2 Rayleigh – Ritz method

The main advantage of Rayleigh-Ritz method with a static beam function as an admissible function is that, it has a capability to solve different boundary conditions in axial direction of a duct. The different axial boundary conditions considered like Simple-Simple (S-S), Clamped-Clamped (C-C), Clamped- Simple (C-S) and Clamped-Free (C-F).

Figure 3 shows the unfold representation of a rectangular duct shown in Fig. 1. It consists of four flat plates connected side by side with intermediate supports and the ends are represented by torsional spring as shown in Fig. 3. Thus, it can be approximated as a beam with three intermediate supports in X_1-direction and another beam in axial direction (z-direction).
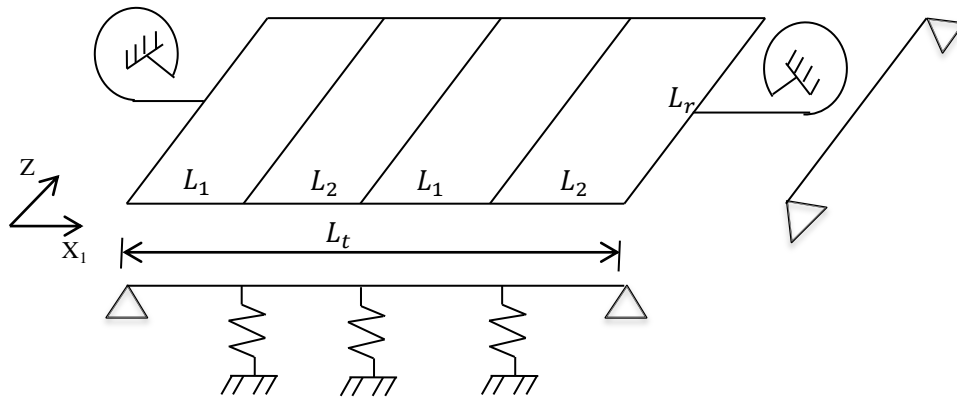
Figure 3: Unfold plate representation of a simply supported rectangular duct

2.2.1 Rayleigh – Ritz Approach

For the free vibration analysis of plate, the deflection w can be expressed as,

$$w(x, y, t) = W(x, y)e^{i\omega t} \tag{17}$$

Where ω is the eigen frequency of plate vibration, t is the time and $i = \sqrt{-1}$

Assuming,

$$\alpha = x / L_t, \quad \beta = z / L_r \tag{18}$$

The modal shape function $W(\alpha, \beta)$ can be expressed in terms of series function as follows,

$$W(\alpha, \beta) = \sum_{m=1}^{\infty} \sum_{n=1}^{\infty} A_{mn} \phi_m(\alpha) \psi_n(\beta) \tag{19}$$

Where, $\phi_m(\alpha)$ and $\psi_n(\beta)$ are the admissible functions in circumferential and axial directions, respectively. A_{mn} are unknown coefficients.

By minimizing the total energy for thin plates as follows,

$$\frac{\partial}{\partial A_{mn}} (U_{max} - T_{max}) = 0 \tag{20}$$

Where, U_{max} and T_{max} are maximum potential and kinetic energies for the thin plates and it can obtained by using the vibration theory of thin plates.

The equation (20) leads to the eigen frequency equation, which is given as,

$$\sum_{m=1}^{\infty}\sum_{n=1}^{\infty}\left[C_{mnij} - \lambda^2 E_{ml}^{(0,0)}F_{nj}^{(0,0)}\right]A_{mn} = 0 \tag{21}$$

Where,

$$C_{mnij} = E_{mi}^{(2,2)}F_{nj}^{(2,2)} + E_{mi}^{(0,0)}F_{nj}^{(2,2)}/\gamma^4 + \mu\left(E_{mi}^{(0,2)}F_{nj}^{(2,0)} + E_{mi}^{(2,0)}F_{nj}^{(0,2)}/\gamma^4\right) + 2(1-\mu)\left(E_{mi}^{(1,1)}F_{nj}^{(1,1)}/\gamma^2\right)$$

$$\lambda^2 = \rho h\,\omega^2 L_r{}^4/H \qquad\qquad\qquad \gamma = L_t/L_r$$

$$E_{mi}^{(r,s)} = \int_0^1 (d^r\phi_m/d\alpha^r)(d^s\phi_i/d\alpha^s)d\alpha \qquad F_{nj}^{(r,s)} = \int_0^1 (d^r\psi_n/d\beta^r)(d^s\psi_j/d\beta^s)d\beta$$

$$\ldots\ldots(22)$$

As discussed, the validity and accuracy of the Rayleigh-Ritz method entirely depends upon the choice of the admissible function. The appropriate admissible function should satisfy at least geometrical boundary conditions and if possible all the boundary conditions. In the presented method, these admissible functions are taken as set of static beam functions. So,

$$\phi_m(\alpha) = y_m(\alpha) \tag{23a}$$

$$\psi_n(\beta) = y_n(\beta) \tag{23b}$$

$y_m(\alpha)$ and $y_n(\beta)$ are the mth and nth static beam functions in X$_1$ and Z directions, respectively. These functions satisfy geometrical boundary conditions and zero deflection condition at the line supports.

2.2.2 Static Beam Functions

The static beam functions for the rectangular plate with three intermediate supports in X$_1$-direction are given in reference [13]. The static beam function in axial direction can be considered as deflection of a beam with end supports [12].

The deflection $y(\alpha)$ of the beam in circumferential direction can be written as

$$y_m(\alpha) = \sum_{k=0}^{3} C_k^m \alpha^k + \sum_{j=1}^{3} P_j^m \frac{(\alpha - \alpha_j)^3}{6} U(\alpha - \alpha_j) + \sin(m\pi\alpha) \tag{24}$$

The deflection $y(\beta)$ of the beam in axial direction can be written as

$$y_n(\beta) = \sum_{k=0}^{3} C_k^n \beta^k + \sin(n\pi\beta) \tag{25}$$

Where,

P_j^m (j= 1, 2, 3) and C_k^n (k= 0, 1, 2, 3) are unknown coefficients, and $U(\alpha - \alpha_j)$ is a Heaviside function.

By observing eq. (24), and eq. (25), the second series term is missing in eq. (25) because the plate is having intermediate supports in the circumferential direction and also continuous in axial direction. Unknowns in these equations can be uniquely decided by using boundary conditions and zero deflection conditions at the intermediate supports. This can be written in the matrix form,

$$\begin{bmatrix} A & D \\ T & G \end{bmatrix} \begin{bmatrix} C^m \\ P^m \end{bmatrix} = \begin{bmatrix} R^m \\ S^m \end{bmatrix} \tag{26}$$

Where, A is $J \times 4$ matrix, T is 4×4 matrix and they refer to the first series terms of equations. D is $J \times J$ matrix, G is $4 \times J$ matrix and they refer to the second series terms of an equation. R^m is $J \times 1$ matrix, S^n is 4×1 matrix and they refer to the third term of the equation for the boundary conditions of the beam.

C^m and P^m are unknown coefficient matrices as follows,

$$C^m = [C_0^m \ C_1^m \ C_2^m \ C_3^m]^T \tag{27a}$$
$$P^m = [P_1^m \ P_2^m \ P_3^m \ ]^T \tag{27b}$$

Generally A, D and R^m matrices are given as,

$$A = \begin{bmatrix} 1 & \alpha_1 & \alpha_1^2 & \alpha_1^3 \\ 1 & \alpha_2 & \alpha_2^2 & \alpha_2^3 \\ \vdots & \vdots & \vdots & \vdots \\ 1 & \alpha_J & \alpha_J^2 & \alpha_J^3 \end{bmatrix}$$

$$R^m = \begin{bmatrix} -\sin(m\pi\alpha_1) \\ -\sin(m\pi\alpha_2) \\ \vdots \\ -\sin(m\pi\alpha_J) \end{bmatrix}$$

$$D = \begin{bmatrix} 0 & 0 & 0 & \cdots & 0 \\ \dfrac{(\alpha_2 - \alpha_1)^3}{6} & 0 & 0 & \cdots & 0 \\ \dfrac{(\alpha_3 - \alpha_1)^3}{6} & \dfrac{(\alpha_3 - \alpha_2)^3}{6} & 0 & \cdots & 0 \\ \vdots & \vdots & \vdots & \vdots & \vdots \\ \dfrac{(\alpha_J - \alpha_1)^3}{6} & \dfrac{(\alpha_J - \alpha_2)^3}{6} & \cdots & \dfrac{(\alpha_J - \alpha_{J-1})^3}{6} & 0 \end{bmatrix} \tag{28}$$

Where, J is the number of intermediate supports which are three in the circumferential direction and zero in axial direction. So in axial direction the matrices A, D, G, R^m and P^m will be zero.

Clamped, simply supported, free boundary conditions are denoted by C, S, F.

The matrix elements T, G and S_i are according to the boundary conditions of the beam, they can be expressed as,

$T_{11}=T_{22}=1$, $S_2^n =-n\pi$ for the beam with C as left end,

$T_{11}=1$, $T_{23}=2$ for the beam with S as left end,

$T_{13}=2$, $T_{24}=6$, $S_2^n =(n\pi)^2$ for the beam with F as left end.

$T_{31} = T_{32} = T_{33} = T_{34} =1$, $T_{42} =1$, $T_{43} =3$, $G_{3j}=(1-\alpha_j)^3/6$, $G_{4j}=(1-\alpha_j)^2/2$, $S_4^n =-n\pi(-1)^n$ for the beam with C as right end,

$T_{31} = T_{32} = T_{33} = T_{34} =1$, $T_{43} =2$, $T_{44} =6$, $G_{3j}=(1-\alpha_j)^3/6$, $G_{4j}=1-\alpha_j$ for the beam with S as right end,

$T_{33}=2$, $T_{34}=6$, $T_{44}=6$, $G_{3j}=1-\alpha_j$, $G_{4j}=1$, $S_4^n = (n\pi)^3(-1)^n$ for the beam with F as right end

2.3 Results and Discussion

To illustrate the validity and the accuracy of proposed analytical methods, some numerical results have been presented and compared with literature results and finite element method (FEM) results. Lack of literature data for the different axial boundary conditions of a rectangular duct, the result of the Rayleigh-Ritz method for the duct with other axial boundary conditions are compared with the results from the FEM analysis. Typical dimensions of duct and material properties used in the calculation are, $L_1=0.4m$, $L_2=0.3m$, $L_r=1.5m$ and thickness $h_r=0.005m$.

For aluminium material properties: Young's modulus E= 71GPa, poisons ratio μ=0. 29, density ρ=2770 kg/m3.

Steel material: E= 210GPa, ρ=7800 kg/m3, μ=0.29.

Square duct of dimensions are 0.14m×0.14m×0.14m. E is 206GPa, ρ=7850kg/m3 and μ=0.3.

There are three parts in the numerical discussion. In the first part, validation of analytical results by comparing with FEM and literature results. Natural frequencies and mode shapes are compared between these methods. In the second part, parametric studies are conducted with respect to different side ratios and aspect ratios. Results are analysed in the tabular form. An attempt made to develop an empirical relations to calculate natural frequencies. In the last part of the discussion, classification of mode shapes according to the symmetric and anti-symmetric conditions are discussed.

2.3.1 Parametric Study

Table 1 to 4 shows comparison of result from different methods for the rectangular duct with aluminium, next four set of tables are for rectangular duct with steel material, and 9th table shows the results for square duct. Results generated in Rayleigh-Ritz method with a static beam admissible function represented by static beam method.

Table 1 : Comparison of first 12 natural frequencies of a rectangular duct with Aluminium material. for S-S boundary conditions

Sr. No.	Static Beam Method	Lee paper[3] Results	Transfer Matrix Method	FEM Results
1	97.97	97.97	97.87	97.87
2	113.16	113.16	113.04	113.03
3	129.81	129.82	125.47	126.81
4	138.76	138.76	138.62	138.59
5	141.41	141.41	140.05	139.88
6	162.35	162.36	161.29	161.16
7	174.97	174.98	174.80	174.75
8	193.47	193.47	187.32	188.87
9	193.95	193.96	193.00	192.87
10	207.38	207.39	205.94	205.50
11	221.89	221.89	221.69	221.60
12	231.03	231.03	229.96	229.68

Table 2 : Comparison of 12 natural frequencies of rectangular duct with Aluminium material for C-C boundary conditions

Sr. No.	Static Beam Method	FEM Results
1	99.27	99.16
2	117.98	117.79
3	130.79	128.32
4	145.27	143.93
5	148.43	148.19
6	170.65	169.54
7	190.19	189.87
8	194.32	191.16
9	207.75	206.68
10	210.75	209.27
11	238.69	236.91
12	243.04	242.52

Table 3: Comparison of 12 natural frequencies of rectangular duct with Aluminium material for C-S boundary conditions

Sr. No.	Static Beam Method	FEM Results
1	98.57	98.46
2	115.39	115.24
3	130.26	127.53
4	143.19	141.76
5	143.34	143.11
6	166.26	165.08
7	182.25	181.95
8	193.87	190.03
9	200.52	199.42
10	208.96	207.30
11	232.44	231.65
12	234.89	233.10

Table 4: Comparison of 12 natural frequencies of rectangular duct with Aluminium material for C-F boundary conditions

Sr. No.	Static Beam Method	FEM Results
1	94.15	93.65
2	104.69	104.30
3	125.83	125.18
4	127.45	-----
5	135.32	132.10
6	152.17	149.67
7	157.74	156.06
8	179.13	176.04
9	190.23	-----
10	199.64	195.98
11	203.89	197.01
12	218.88	212.87

Table 1 shows the results comparison of different methods for aluminium rectangular duct. As mentioned earlier Rayleigh-Ritz method with static beam functions as admissible functions is capable to incorporate other boundary conditions. These results are compared with FEM analysis results. Tables 2, 3 and 4 shows comparison of the results for the different boundary conditions like C-C, C-S and C-F respectively for the aluminium rectangular duct. Similarly, the results are generated for the steel rectangular duct and for the square duct. It is observed that the results are in good agreement between two methods.

Figure 4 shows some of the mode shapes for the aluminium rectangular ducts.
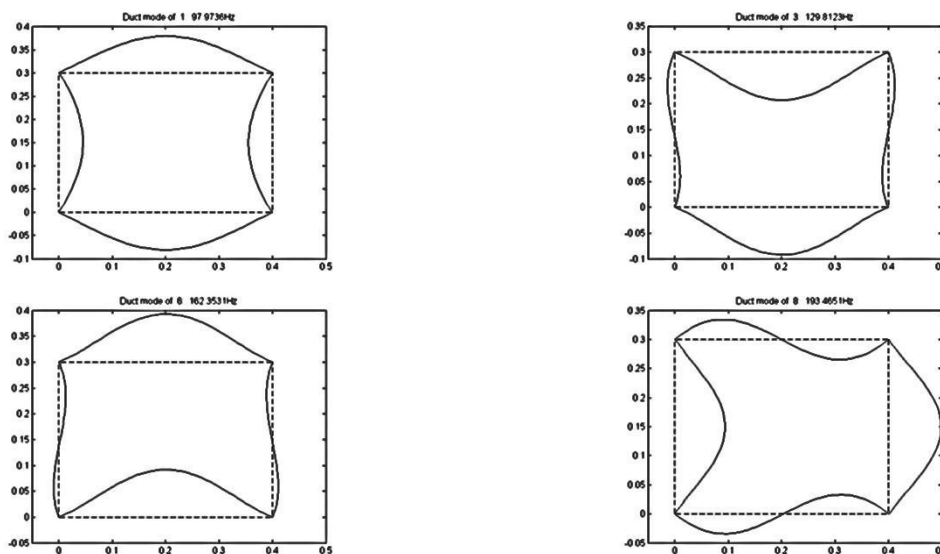

Figure 4: Mode shapes for 1, 3, 6 and 8th natural frequency of Al rectangular duct

Table 5: Comparison of 12 natural frequencies of a rectangular duct with steel for S-S boundary conditions

Sr. No.	Static Beam Method	Lee paper Results	Transfer Matrix Method	FEM Results
1	100.41	100.41	100.31	100.23
2	115.98	115.98	115.86	115.65
3	133.04	133.04	128.60	130.03
4	142.22	142.22	142.07	141.58
5	144.93	144.93	143.53	143.14
6	166.39	166.39	165.30	164.62
7	179.33	179.33	179.15	178.2
8	198.28	198.28	191.98	193.96
9	198.78	198.78	197.80	196.66
10	212.54	212.54	211.07	210.39
11	227.41	227.41	227.21	225.68
12	236.77	236.77	235.68	234.65

Table 6 : Comparison of 12 natural frequencies of rectangular duct with Al for C-C boundary conditions

Sr. No.	Static Beam Method	FEM Results
1	101.74	101.53
2	120.91	120.45
3	134.04	131.32
4	148.88	147.14
5	152.12	151.28
6	174.90	173.05
7	194.92	193.57
8	199.16	195.68
9	212.92	210.67
10	216.00	213.96
11	244.09	241.76
12	248.90	247.08

Table 7: Comparison of 12 natural frequencies of rectangular duct with Al for C-S boundary conditions

Sr. No.	Static Beam Method	FEM Results
1	101.02	100.82
2	118.27	117.88
3	133.50	130.63
4	146.76	145.00
5	146.90	146.16
6	170.40	168.58
7	186.78	185.54
8	198.69	194.79
9	205.51	203.33
10	214.16	212.09
11	237.79	236.00
12	240.26	238.04

Tables 5- 8 have the results for steel rectangular duct and Table 9 for the square duct. Table 5 shows the comparison of natural frequencies calculated from different methods for a rectangular duct with steel material. The results are in good agreement with FEM results and also literature data.

Table 8: Comparison of 12 natural frequencies of a rectangular duct with steel for C-F boundary conditions

Sr. No.	Static Beam Method	FEM Results
1	96.50	95.83
2	107.35	105.73
3	129.29	125.42
4	130.64	--
5	139.00	134.42
6	156.04	151.11
7	161.74	155.03
8	187.27	176.22
9	194.98	194.79
10	204.79	199.71
11	209.32	211.73
12	225.21	220.05
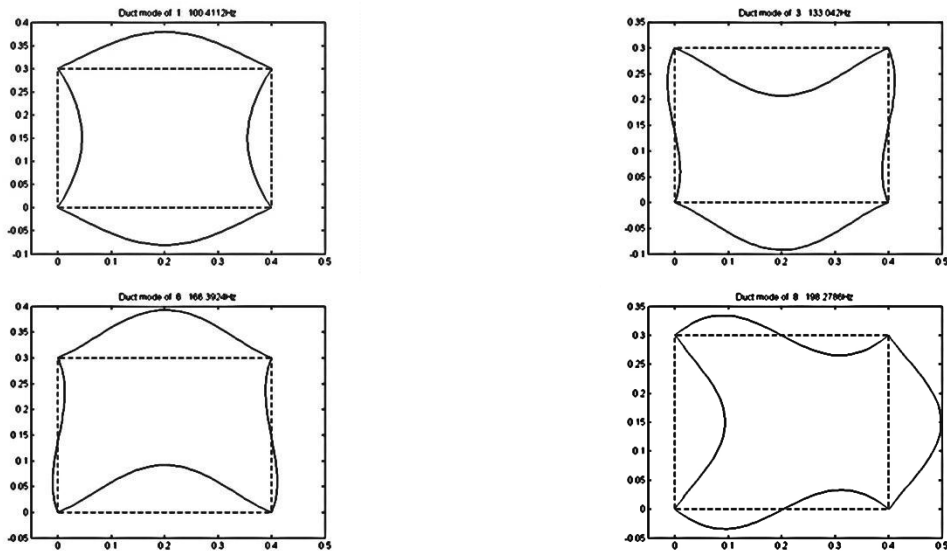
Figure 5: Mode shapes for 1, 3, 6 and 8th natural frequency of steel rectangular duct

Figure 4 and 5 shows the mode shapes for the 1, 3, 6 and 8th natural frequencies of the Al and steel rectangular ducts. One can clearly observe from these figures that, as the dimensions of both the ducts are same the mode shapes for the respective natural frequencies are similar. Modes shown are symmetric – symmetric, symmetric – antisymmetric, symmetric – antisymmetric, antisymmetric – antisymmetric respectively.

Table 9 : Comparison of first 12 natural frequencies of a square duct for S-S boundary conditions

Sr. No.	Static Beam Method	Receptance method Azmi et al. [1]	Transfer Matrix method	LEE Paper[3]	Sai Jagan Mohan Rudra Pratap[5]
1	487.02	487.04	432.62	487.01	485.8
2	583.42	583.51	582.84	583.48	582.03
3	587.46	583.51	582.84	589.78	582.03
4	720.59	714.27	634.08	724.61	713.04
5	1217.50	1217.60	1199.30	1217.50	1222.80
6	1217.50	1217.60	1215.90	--	1224.51
7	1274.90	1274.80	1274.30	--	1281.33
8	1278.62	1274.80	1274.30	--	1281.36
9	1356.20	1350.60	--	--	1356.52
10	1447.00	1447.10	1444.71	1447.5	--
11	1460.70	--	1444.70	1468.8	--
12	1729.31	1705.90	1701.83	1742.8	1715.70

Some of the values in the above table are shown as '--' because these values are not predicted by those methods.
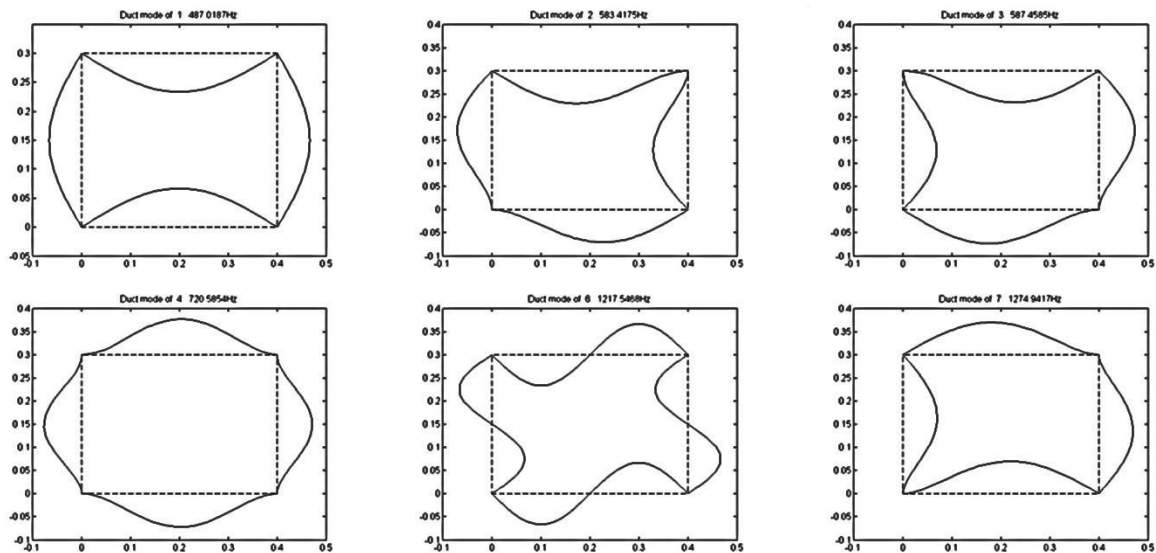

Figure 6: Mode shapes for 1, 2, 3, 4, 6 and 7th natural frequency of a square duct

Figure 6 shows the mode shapes of a square duct. The dominance of symmetrical modes can be observed in natural frequency and mode shapes.

2.3.2 Classification of Mode Shapes

The aim of this classification is to show that how the mode shapes of a complex structure like rectangular duct can be characterized by using simple features of vibration of plate pairs. Table 10 shows the first 29 natural frequencies of non-rigid body modes for an aluminium rectangular duct with S-S boundary conditions. These modes cover the frequency range up to 400 Hz. These modes are classified into four groups according to the symmetric and anti-symmetric properties between the plate pairs. The rectangular ducts consist of 2 plate pairs, each in X and Y direction i.e. at X=0 and $X=L_1$, Y=0 and $Y=L_2$

Table 10: Classification of first 29 modes of a rectangular duct

Group	Duct Modes
(D_S,S)	[D_S(1,1),S(1,1)]97.97Hz [D_S(1,2),S(1,2)]113.16Hz [D_S(1,3),S(1,3)]138.76Hz [D_S(1,4),S(1,4)]174.97Hz [D_S(1,5),S(1,5)]221.89Hz [S(1,1)*,D_S(1,1)]248.31Hz [S(1,2)*,D_S(1,2)]258.69Hz [S(1,3)*,D_S(1,3)]277.15Hz [D_S(1,6),S(1,6)]279.55Hz [S(1,4)*,D_S(1,4)]304.98Hz [S(1,5)*,D_S(1,5)]343.35Hz [S(1,6)*,D_S(1,6)*]347.96Hz [S(1,6)*,D_S(1,6)]393.04Hz
(D_AS,S)	[D_AS(1,1),S(2,1)]129.81Hz [D_AS(1,2),S(2,2)]141.41Hz [D_AS(1,3),S(2,3)]162.35Hz [D_AS(1,4),S(2,4)]193.95Hz [D_AS(1,5),S(2,5)]236.93Hz [D_AS(1,6),S(2,6)]291.47Hz [D_AS(1,7)*,AS(2,6)*]357.5Hz
(S,D_AS)	[S(2,1),D_AS(1,1)]193.47Hz [S(2,2),D_AS(1,2)]207.38Hz [S(2,3),D_AS(1,3)]231.03Hz [S(2,4),D_AS(1,4)]264.85Hz [S(2,5),D_AS(1,5)]309.23Hz
(D_AS,AS)	[D_AS(2,1),AS(2,1)]360.5Hz [AS(2,6),D_AS(1,6)]364.41Hz [D_AS(2,2),AS(2,2)]375.43Hz [D_AS(2,3),AS(2,3)]400.45Hz

The distribution between the pair is symmetric, if the phase and amplitude of plates in one pair is same (i.e. both plates oscillates inward and outward with equal amplitude at same instance). The distribution is anti-symmetric, if the phase between the plates of same pair is opposite (i.e. if the one plate moves inward then another plate of the pair move outward). These symmetric and antis-

symmetric properties can be easily seen in the Figures 4 and 5 where the mode shapes have been plotted in 2D. The dominating pair can be identified by comparing the amplitude between the plate pairs.

Mode shape structure can be described as

1. Symmetrical property of each pair,
2. Vibration pattern in each pair,
3. Identification of dominating pair between plate pairs, and
4. The corresponding natural frequency.

Out of plane vibration in the respective modes is described by using two numbers. These numbers are decided by using the number of antinodes present in X and Y direction respectively.

Figures 7 and 8 are the graphical representation of the mode shapes. The contours plot the amplitude distribution in the plate pairs. The isometric view and the 2D views are plotted for 1st and 12th modes . The isometric views are useful for the phase relations.

Notation used in classification of these duct modes as [D_S (1,1), S (1,1)] 97.97 Hz. It represents natural frequency 97.97Hz having the symmetric properties and the first pair that is pair in X direction is dominating with respect to the amplitude. It can be clearly seen in the Figure 7 (b and c) where isometric view and 2D view for this natural frequency is plotted. The numbers (1, 1) for first pair shows that the number of antinodes for X=0 plate and for X=L$_1$ plate is '1' and same '1' number of antinodes in Y direction plate pairs. This can be seen in the Figure 7(a) i. e in the contour plots of the mode shape

Y=0

X=0

Y=0.3

X=0.4
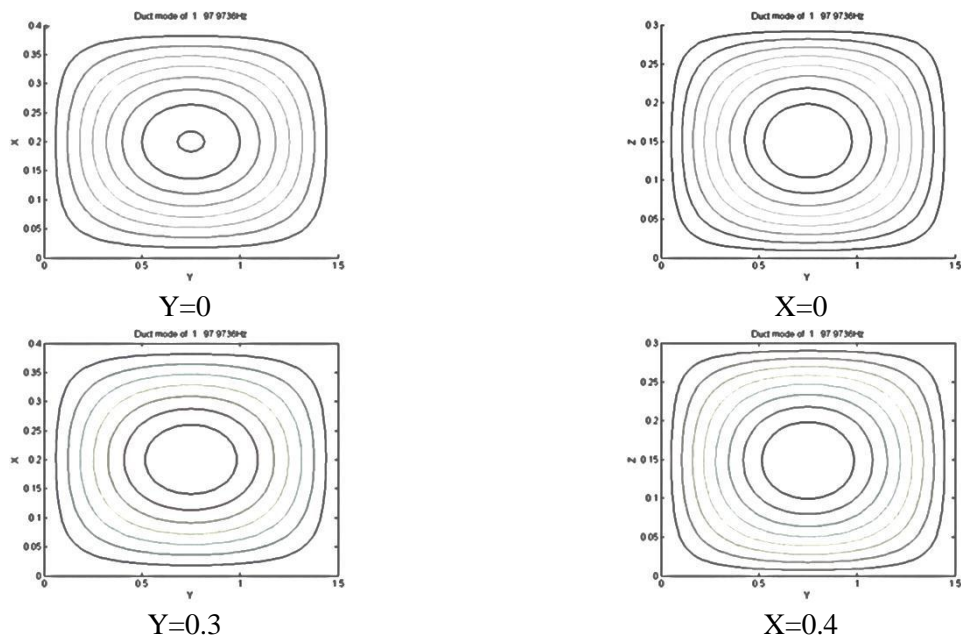
(a)
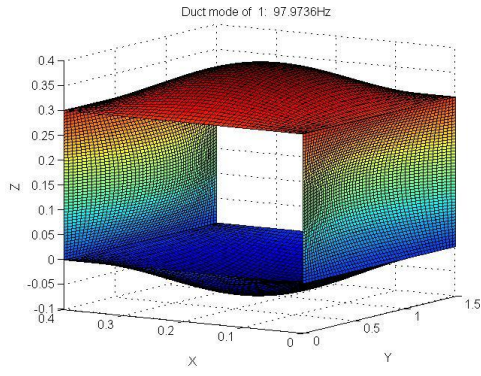
(b)
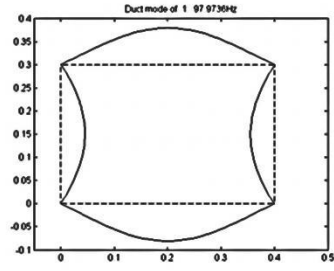
(c)

Figure 7: Mode shape distribution of mode [D_S(1,1),S(1,1)]₉₇.₉₇₄Hz (a) Contour Plot (b) Isometric View (c) 2D plot

Consider the mode natural frequency 231.03Hz which is given (s [S, 2,3) (D_AS] 1,3)]231.03Hz. This says that the pair in X – direction is symmetric and the pair in Y- direction having the anti-symmetric properties, and the pair in Y direction is dominating with respect to the amplitude. This can be clearly seen in the Figure 8(b and c) where isometric view and 2D view for this natural frequency is plotted. The numbers (2, 3) for first pair shows that the number of antinodes for X=0 plate is '2' and for X=L_1 plate is '3', and '1' and '3'numbers of antinodes in Z direction plate pairs for the Y=0 and Y=L_2 plates, respectively. This can be seen in the Figure 8(a) i. e in the contour plots of the mode shape

Y=0

X=0

Y=0.3

X=0.4

(a)

Duct mode of 12: 231.0266Hz

(b)

Duct mode of 12 231.0266Hz

(c)
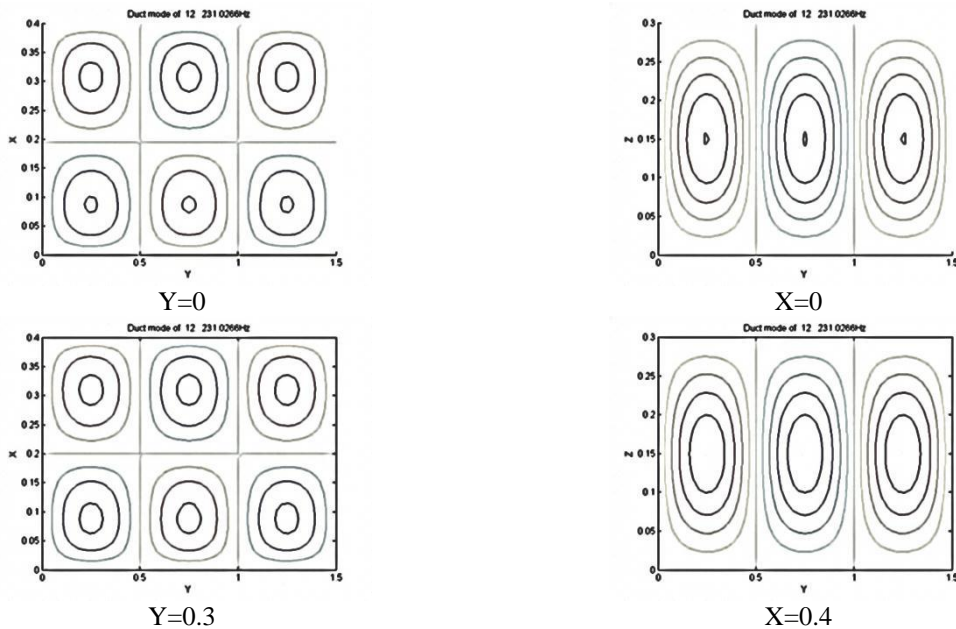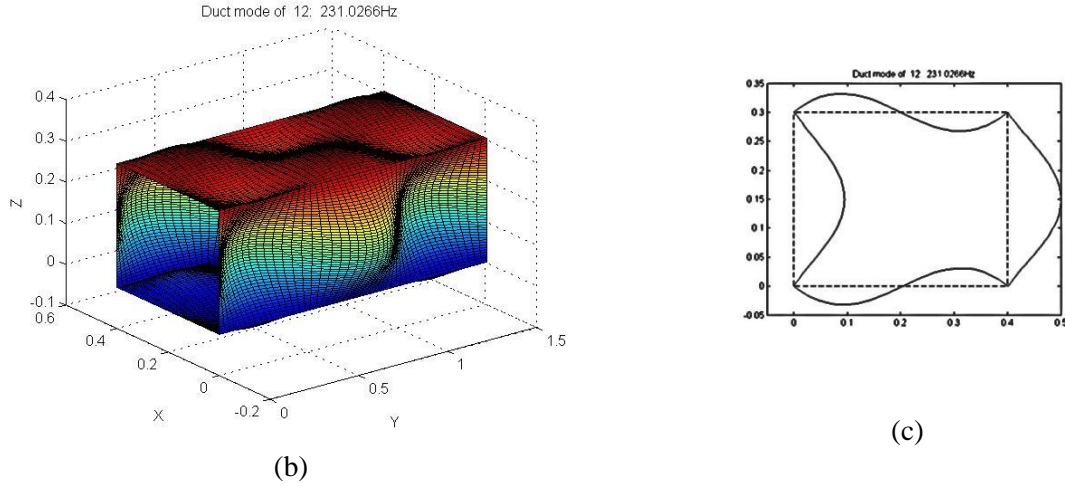
Figure 8: Mode shape distribution of mode [S(2,3),D_AS(1,3)]$_{231.03Hz}$ (a) Contour Plot (b) Isometric View (c) 2D plot

2.3.3   Engineering Data

Now this validated analytical model is used to generate values of non-dimensional frequency parameter (λ) for different standard dimensions of the rectangular ducts. Dimensions of ducts divided into two ratios, one is side ratio and represented by 'S$_1$'. The other one is aspect ratio and represented by 'S$_2$' .The non-dimensional frequency (λ) values have been given for the different combinations of these ratios. The ratios used are 0.25, 0.5, 0.75 and 1. According to the dimension of the duct one has to decide both the ratios, then from the table select the appropriate λ value for the combination of these ratios. Equation (29) can be used to calculate the natural frequencies in Hz from this non dimensional value. This non dimensional frequency parameter is independent of the material properties except the poisons ratio which is used as 0.29 to generate these values.

Frequency (*f*) in Hz is given by,

$$f = \frac{\lambda}{2\pi \times L_t{}^2} \sqrt{\frac{E h_r^2}{12\rho(1 - \mu^2)}} \tag{29}$$

Table 11 to 14 contains the values of λ for first four natural frequencies of rectangular duct. This data generated for different combinations of aspect ratios and side ratios and also for different axial boundary conditions like S-S, C-C, C-S and C-F respectively.

21

Table 11: Non-dimensional frequency parameter (λ) for S-S axial boundary condition

Mode no.	$\downarrow S_1$ $S_2 \rightarrow$	0.25	0.5	0.75	1
1		1678.81	424.56	192.37	111.19
2	0.25	1698.35	444.75	213.57	130.32
3		1731.41	480.53	227.03	133.55
4		1779.04	503.55	245.79	150.33
1		2066.62	522.62	236.72	1 6.69
2	0.5	2090.51	546.78	261.36	161.90
3		2130.53	588.06	295.12	168.77
4		2187.11	647.61	304.25	189.31
1		2409.82	609.41	276.02	159.34
2	0.75	2437.71	637.34	304.05	187.50
3		2484.11	684.12	351.20	211.54
4		2549.40	750.01	370.74	233.18
1		2536.54	641.52	290.61	167.78
2	1	2566.14	671.13	320.21	197.39
3		2615.41	720.48	369.56	246.74
4		2684.52	789.57	438.65	254.14

Table 12: Non-dimensional frequency parameter (λ) for C-C axial boundary condition

Frequency no.	$\downarrow S_1$ $S_2 \rightarrow$	0.25	0.5	0.75	1
1		1679.71	426.02	194.49	114.12
2	0.25	1701.64	450.18	221.69	132.86
3		1739.22	492.66	228.86	144.41
4		1790.91	504.81	252.95	160.12
1		2067.81	524.15	238.81	139.48
2	0.5	2094.34	552.26	269.08	171.01
3		2139.32	600.20	296.77	171.96
4		2200.11	657.45	320.45	197.92
1		2411.15	611.05	278.14	162.07
2	0.75	2441.91	643.01	311.65	197.15
3		2494.03	696.64	367.04	213.58
4		2563.62	769.22	372.31	240.96
1		2537.91	643.21	292.76	170.52
2	1	2570.52	676.93	327.85	206.98
3		2625.82	733.28	385.44	256.09
4		2699.31	808.97	447.52	261.29

Table 13: Non-dimensional frequency parameter (λ) for C-S axial boundary condition

Frequency no.	$S_2 \rightarrow$ $\downarrow S_1$	0.25	0.5	0.75	1
1		1679.23	425.22	193.32	112.46
2	0.25	1700.02	447.36	217.33	131.43
3		1735.07	486.24	227.84	138.50
4		1784.83	504.12	249.11	154.78
1		2067.24	523.31	237.67	137.9
2	0.5	2092.51	549.47	265.01	166.55
3		2134.62	593.78	295.86	169.76
4		2193.55	656.79	311.88	193.27
1		2410.47	610.15	276.98	160.56
2	0.75	2439.91	640.18	307.70	192.02
3		2488.83	690.04	358.68	212.45
4		2556.35	759.26	371.44	236.80
1		2537.11	642.28	291.58	169.01
2	1	2568.42	674.05	323.90	201.91
3		2620.36	726.50	377.07	255.02
4		2691.81	798.94	446.67	255.68

Table 14: Non-dimensional frequency parameter (λ) for C-F axial boundary condition

Frequency no.	$S_2 \rightarrow$ $\downarrow S_1$	0.25	0.5	0.75	1
1		1673.84	419.56	187.35	106.12
2	0.25	1687.01	433.38	201.87	121.26
3		1714.45	462.46	222.62	125.87
4		1777.71	499.18	232.96	139.24
1		2060.52	516.49	230.60	130.58
2	0.5	2076.94	533.24	247.76	148.15
3		2109.71	567.12	282.94	164.01
4		2152.16	616.66	290.38	177.96
1		2402.53	602.24	268.88	152.23
2	0.75	2419.63	621.66	288.55	172.15
3		2450.82	660.51	327.82	206.34
4		2506.91	719.04	365.55	211.42
1		2528.80	633.90	283.02	160.24
2	1	2549.34	654.50	303.83	181.26
3		2590.37	695.72	345.11	222.43
4		2651.32	756.99	407.09	248.42

2.3.4 Empirical Relation

In the above section, the non-dimensional frequency parameter (λ) has been given for different duct geometry dimensions. From which one can calculate the first four natural frequencies directly for standard duct dimensions. In this section, the empirical relation has been presented which

will be useful to get the non-dimensional frequency parameter (λ) for any combination of aspect ratio between (0.25 to 1) and side ratio between (0.25 to 1). This empirical relation has been formed by performing curve fitting of the above generated data. The empirical relation is of the form,

$$\lambda = \lambda_0 \times S_1^{0.31} \times S_2^{-1.96} \tag{30}$$

Where, λ_0 is a constant which depends on the axial boundary condition. Table 15 represents the values of constant 'λ_0' for different cases.

Table 15: Values of constant 'λ_0' in empirical equation

Axial boundary condition	Value of constant 'A'
S-S	169
C-C	171.5
C-S	170
C-F	165

This empirical relation is useful for calculating the first fundamental frequency of a rectangular duct with different axial boundary conditions. It is observed from Equation (30) and also Tables (11-14) that fundamental natural frequency is sensitive to aspect ratio compared to side ratio.

Chapter 3

Flat Oval Duct

Other than rectangular duct there are other shapes of ducts i.e. circular and flat oval which is also extensively used in heating ventilation and air conditioning units (HVAC) for the air handling purpose. This chapter explains analytical method which can be used for natural frequency calculation for flat oval duct. As this analysis starts with a theory of shells, natural frequency calculations for curved plates and cylindrical ducts is also discussed.

3.1   Transfer Matrix Method

As there are advantages of using the transfer matrix method over another method as mentioned in previous chapters, the transfer matrix method is chosen for free vibration analysis of flat oval ducts. Analysis started with the free vibration equation of shells with simply supported boundary conditions. The transfer matrix for the circular plates has been derived from shell governing equations. Free vibration of curved plates and cylindrical ducts are explained by using this transfer matrix. Transfer matrix for elliptical duct is a combination of circular plate transfer matrix, point matrix and flat plate transfer matrix.

From the Goldenveizer-Novozhilov equations of free vibration of the shells, equilibrium equations and the components of forces can be written as follows,

$$\frac{\partial N_x}{\partial x} + \frac{\partial N_{sx}}{\partial s} + \rho H \omega^2 u = 0$$

$$\frac{\partial N_s}{\partial s} + \frac{\partial N_{xs}}{\partial x} + \frac{Q_s}{R} + \rho H \omega^2 v = 0$$

$$\frac{\partial Q_x}{\partial x} + \frac{\partial Q_s}{\partial s} + \frac{N_s}{R} + \rho H \omega^2 w = 0$$

$$(31)$$

$$Q_x = \frac{\partial M_s}{\partial x} + \frac{\partial M_{sx}}{\partial s} \quad , \qquad Q_s = \frac{\partial M_s}{\partial s} + \frac{\partial M_{xs}}{\partial x} \tag{32}$$

$$S_s = Q_s + \frac{\partial M_{sx}}{\partial x} \tag{33}$$

$$N_s = D\left\{\frac{\partial u}{\partial x} + \mu\left(\frac{\partial v}{\partial s} + \frac{w}{R}\right)\right\} , \quad N_s = D\left(\frac{\partial v}{\partial s} + \frac{w}{R} + \mu\frac{\partial u}{\partial x}\right)$$

$$N_{xs} = \frac{D(1-\mu)}{2}\left\{\frac{\partial u}{\partial s} + \frac{\partial v}{\partial x} + \frac{H^2}{6R}\frac{\partial}{\partial x}\left(\frac{v}{R} - \frac{\partial w}{\partial s}\right)\right\}$$

$$N_{sx} = \frac{D(1-\mu)}{2}\left(\frac{\partial u}{\partial s} + \frac{\partial v}{\partial x}\right)$$

$$M_x = K\left\{-\frac{\partial^2 w}{\partial x^2} + \mu\frac{\partial}{\partial s}\left(\frac{v}{R} - \frac{\partial w}{\partial s}\right)\right\}$$

$$M_s = K\left\{\frac{\partial}{\partial s}\left(\frac{v}{R} - \frac{\partial w}{\partial s}\right) - \mu\frac{\partial^2 w}{\partial x^2}\right\}$$

$$M_{xs} = M_{sx} = K(1-\mu)\frac{\partial}{\partial x}\left(\frac{v}{R} - \frac{\partial w}{\partial s}\right) \tag{34}$$

$$\psi = \frac{v}{R} - \frac{\partial w}{\partial s} \quad , \qquad D = Eh/(1-\mu^2), \quad K = Eh/12(1-\mu^2) \tag{35}$$

For the simply supported axial boundary conditions one can assume the state space variables in the form,

$$u = (1/K)\,\bar{u}\cos\delta x \qquad v = (1/K)\bar{v}\sin\delta x$$

$$w = (1/K)\bar{w}\sin\delta x \qquad \psi = (\delta/K)\bar{\psi}\sin\delta x$$

$$M_s = \delta^2\overline{M_s}\sin\delta x \qquad S_s = \delta^3\overline{S_s}\sin\delta x$$

$$N_s = \delta^3\overline{N_s}\sin\delta x \qquad N_{sx} = \delta^3\overline{N_{sx}}\cos\delta x \tag{36}$$

Where, $\delta = (m \times \pi)/L$, m is mode number in axial direction and L is the length of shell.

By simplifying equations (31-35) and also substituting equation (36) in simplified equations provides the equations of vibration in matrix differential form as follows,

$$d/ds\begin{Bmatrix} \overline{w} \\ \overline{\psi} \\ \overline{M}_s \\ \overline{S}_s \\ \overline{v} \\ \overline{u} \\ \overline{N}_s \\ \overline{N}_{sx} \end{Bmatrix} = \begin{bmatrix} 0 & -\delta & 0 & 0 & \dfrac{1}{R} & 0 & 0 & 0 \\ -\mu\delta & 0 & \delta & 0 & 0 & 0 & 0 & 0 \\ 0 & 2\alpha(1-\mu) & 0 & \delta & 0 & 0 & 0 & 0 \\ A_{41} & 0 & \mu\delta & 0 & 0 & 0 & \dfrac{1}{R} & 0 \\ -\dfrac{1}{R} & 0 & 0 & 0 & 0 & \mu\alpha & \dfrac{\delta^3 K}{D} & 0 \\ 0 & 0 & 0 & 0 & -\dfrac{m\pi}{l} & 0 & 0 & \dfrac{2K\delta^3}{D(1-\mu)} \\ 0 & 0 & 0 & -\dfrac{1}{R} & -\dfrac{\rho h\omega^2}{\delta^3 K} & 0 & 0 & \alpha \\ 0 & 0 & 0 & 0 & 0 & A_{86} & -\mu\delta & 0 \end{bmatrix} \begin{Bmatrix} \overline{w} \\ \overline{\psi} \\ \overline{M}_s \\ \overline{S}_s \\ \overline{v} \\ \overline{u} \\ \overline{N}_s \\ \overline{N}_{sx} \end{Bmatrix} \quad (37)$$

Where,

$$A_{41} = -\frac{\rho h\omega^2}{\delta^3 K} + \alpha(1-\mu^2) \quad and \quad A_{86} = \frac{D(1-\mu^2)}{K\delta} - \frac{\rho h\omega^2}{K\delta^3}$$

The above equation can also be written as,

$$\left(\frac{d}{dS}\right)Z(S_1) = [\mathbf{A}] * Z(S_0) \tag{38}$$

$Z(S)$ is state vector which can also be expressed as,

$$Z(S_1) = \mathbf{T(S, S_o)} * Z(S_0) \tag{39a}$$

By substituting equation (39 a) in to equation (38) we get,

$$\left(\frac{d}{dS}\right)\mathbf{T(S, S_0)} = [\mathbf{A}]\mathbf{T(S, S_0)} \tag{39b}$$

Where,

$\mathbf{T(S, S_o)}$ represents the Transfer Matrix, which relates space vectors at S_0 to S_1. The transfer matrix elements are calculated by using Runge-Kutta-Gill integration method. In the same way if we substitute radius of curvature, R as infinite in equation 37, provides a transfer matrix for flat plate.

The final transfer matrix size for plate or shell will be of 8×8 so it has 8 state space variables. The transfer matrix is similar to the rectangular transfer matrix as discussed in chapter 2.

3.1.1 Curved Plates

Figure 9 shows curved plate with boundary condition notations. There are four boundaries on curved plates, two other in the axial direction and two in the circumferential direction. Only simple supported boundary conditions in the axial direction are considered for transfer matrix analysis. Different boundary conditions can be applied in the circumferential direction. These boundary conditions are defined as,
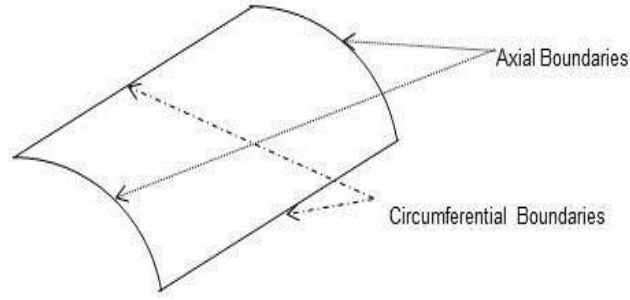
Figure 9: Schematic diagram of curved plate

Simple support: $u = w = M_s = N_s = 0$ (40a)

Clamped Support: $u = v = w = \psi = 0$ (40b)

 Free end: $M_s = N_s = S_s = N_{sx} = 0$ (40c)

By using these boundary conditions, 8×8 transfer matrix will be reduced to 4×4 matrix .The only unknown parameter is frequency parameter. By solving these matrices as eigenvalue problem, one can get natural frequency and mode shapes for the respective boundary condition. The final forms of transfer matrices for different boundary conditions are,

For Simple-Simple support:

$$\begin{bmatrix} T_{12} & T_{14} & T_{15} & T_{18} \\ T_{32} & T_{34} & T_{35} & T_{38} \\ T_{62} & T_{64} & T_{65} & T_{68} \\ T_{72} & T_{74} & T_{75} & T_{78} \end{bmatrix} \begin{bmatrix} \psi \\ S_s \\ v \\ N_{sx} \end{bmatrix}_{S=S_0} = 0 \tag{41}$$

For clamped-clamped support:

$$\begin{bmatrix} T_{13} & T_{14} & T_{17} & T_{18} \\ T_{23} & T_{24} & T_{27} & T_{28} \\ T_{53} & T_{54} & T_{57} & T_{58} \\ T_{63} & T_{64} & T_{67} & T_{68} \end{bmatrix} \begin{bmatrix} M_s \\ S_s \\ N_s \\ N_{sx} \end{bmatrix}_{S=S_0} = 0 \tag{42}$$

For free-free boundary conditions:

$$\begin{bmatrix} T_{31} & T_{32} & T_{35} & T_{36} \\ T_{41} & T_{42} & T_{45} & T_{46} \\ T_{71} & T_{72} & T_{75} & T_{76} \\ T_{81} & T_{82} & T_{85} & T_{86} \end{bmatrix} \begin{bmatrix} w \\ \psi \\ v \\ u \end{bmatrix}_{S=S_0} = 0 \tag{43}$$

For Clamped-Simply supported:

$$\begin{bmatrix} T_{12} & T_{14} & T_{15} & T_{18} \\ T_{22} & T_{24} & T_{25} & T_{28} \\ T_{52} & T_{54} & T_{55} & T_{58} \\ T_{62} & T_{64} & T_{65} & T_{68} \end{bmatrix} \begin{bmatrix} \psi \\ S_s \\ v \\ N_{sx} \end{bmatrix}_{S=S_0} = 0 \tag{44}$$

For Clamped-Free:

$$\begin{bmatrix} T_{11} & T_{12} & T_{15} & T_{16} \\ T_{21} & T_{22} & T_{25} & T_{26} \\ T_{51} & T_{52} & T_{55} & T_{56} \\ T_{61} & T_{62} & T_{65} & T_{66} \end{bmatrix} \begin{bmatrix} w \\ \psi \\ v \\ u \end{bmatrix}_{S=S_0} = 0 \tag{45}$$

For Simple-Free:

$$\begin{bmatrix} T_{11} & T_{12} & T_{15} & T_{16} \\ T_{31} & T_{32} & T_{35} & T_{36} \\ T_{61} & T_{62} & T_{65} & T_{66} \\ T_{71} & T_{72} & T_{75} & T_{76} \end{bmatrix} \begin{bmatrix} w \\ \psi \\ v \\ u \end{bmatrix}_{S=S_0} = 0 \tag{46}$$

After getting frequency parameter (λ) natural frequency can be calculated by using the following formula,

$$f = \left[\lambda/2\pi R_{cp}\right]\sqrt{E/\rho(1-\mu^2)} \tag{47}$$

Mode shapes can be calculated by re-substituting λ in above matrices and calculating eigen vectors for the problem.

3.1.2 Circular Duct

Transfer matrix derived for curved plate can be used for vibration analysis of circular ducts. For this analysis a quarter section of circular duct is considered with symmetrical boundary conditions at two ends. Figure 10 shows circular duct and its corresponding quarter section. Symmetric boundary conditions and final (4×4) matrices after reducing from (8×8) are given as follows. These boundary conditions are same as used for rectangular ducts only final matrices differs this because of different orientation of state space matrix.
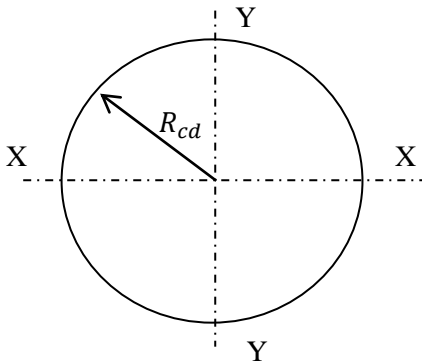
Figure 10(a): Circular duct cross-section   **Figure 10(b): Quarter section of a circular duct**
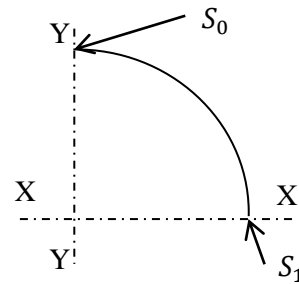
Symmetrical boundary conditions at symmetrical plane written as,

$v = \psi = S_s = N_{sx} = 0$ for Symmetric(S) mode   (48a)

$u = w = M_s = N_s = 0$ for Anti-Symmetric (AS) mode.   (48b)

S-S mode:

$$\begin{bmatrix} T_{21} & T_{23} & T_{26} & T_{27} \\ T_{41} & T_{43} & T_{46} & T_{47} \\ T_{51} & T_{53} & T_{56} & T_{57} \\ T_{81} & T_{83} & T_{86} & T_{87} \end{bmatrix} \begin{bmatrix} w \\ M_s \\ u \\ N_s \end{bmatrix}_{S=S_0} = 0 \tag{49}$$

AS-S mode:

$$\begin{bmatrix} T_{22} & T_{24} & T_{25} & T_{28} \\ T_{42} & T_{44} & T_{45} & T_{48} \\ T_{52} & T_{54} & T_{55} & T_{58} \\ T_{82} & T_{84} & T_{85} & T_{88} \end{bmatrix} \begin{bmatrix} \psi \\ S_s \\ v \\ N_{sx} \end{bmatrix}_{S=S_0} = 0 \tag{50}$$

S-AS mode:

$$\begin{bmatrix} T_{11} & T_{13} & T_{16} & T_{17} \\ T_{31} & T_{33} & T_{36} & T_{37} \\ T_{61} & T_{63} & T_{66} & T_{67} \\ T_{71} & T_{73} & T_{76} & T_{77} \end{bmatrix} \begin{bmatrix} w \\ M_s \\ u \\ N_s \end{bmatrix}_{S=S_0} = 0 \tag{51}$$

AS-AS mode:

$$\begin{bmatrix} T_{12} & T_{14} & T_{15} & T_{18} \\ T_{32} & T_{34} & T_{35} & T_{38} \\ T_{62} & T_{64} & T_{65} & T_{68} \\ T_{72} & T_{74} & T_{75} & T_{78} \end{bmatrix} \begin{bmatrix} \psi \\ S_s \\ v \\ N_{sx} \end{bmatrix}_{S=S_0} = 0 \tag{52}$$

The frequency parameter λ is unknown which can be determined by calculating eigenvalues of these matrices. The natural frequencies are obtained by the following equation,

$$f = [\lambda/2\pi R_{cd}]\sqrt{E/\rho(1-\mu^2)} \tag{53}$$

Mode shapes can be obtained by back substituting the values of λ in the equations 49-52 and calculating eigen vectors.

3.1.3 Flat Oval Duct

Figure 11 (a) shows a cross-section of flat oval duct consisting of two half circles and two flat plates. For transfer matrix analysis, only quarter section of this duct is considered. The total transfer matrix for this quarter section can be obtained by multiplying one transfer matrix for curved plate and one for flat plate with point matrix to define joint properties between flat and circular plates.

So the total transfer matrix to relate the space variable at $S = S_0$ to $S = S_1$ of quarter section of flat oval duct (shown in fig. 11b) can be written as follows
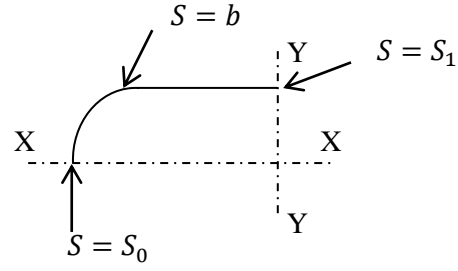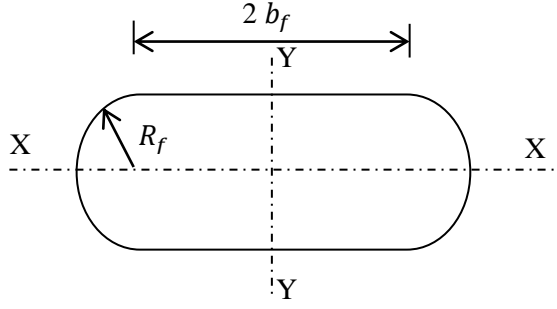
Figure 11(a): Cross section of flat oval duct   **Figure 11(b): Quarter section of flat oval duct**

$$Z(S) = \begin{cases} \mathbf{T(b, S_0)}Z(S)|_{S=S_0} & (S < b) \\ \mathbf{T(S_1, b)PT(b, S_0)}Z(S)|_{S=S_0} & (S > b) \end{cases} \tag{54}$$

Where,

$\mathbf{T(b, S_0)}$ is the transfer matrix for the circular plate, $\mathbf{T(S_0, b)}$ is the transfer matrix for the flat plate. And $\mathbf{P}$ is point matrix which is defined as,

$$\mathbf{P} = \begin{bmatrix} 1 & 0 & 0 & 0 & 0 & 0 & 0 & 0 \\ 0 & -\text{Cos}[\xi] & -\text{Sin}[\xi] & 0 & 0 & 0 & 0 & 0 \\ 0 & \text{Sin}[\xi] & -\text{Cos}[\xi] & 0 & 0 & 0 & 0 & 0 \\ 0 & 0 & 0 & 1 & 0 & 0 & 0 & 0 \\ 0 & 0 & 0 & 0 & 1 & 0 & 0 & 0 \\ 0 & 0 & 0 & 0 & 0 & -\text{Cos}[\xi] & -\text{Sin}[\xi] & 0 \\ 0 & 0 & 0 & 0 & 0 & \text{Sin}[\xi] & -\text{Cos}[\xi] & 0 \\ 0 & 0 & 0 & 0 & 0 & 0 & 0 & 1 \end{bmatrix} \tag{55}$$

Where, ξ is the angle between the circular plate and the flat plate.

The total transfer matrix is a 8×8 matrix which will reduce to 4×4 after applying the symmetrical boundary conditions. These boundary conditions and final matrices are same as given for circular duct in equations (49-52).

The frequency parameter λ is unknown which can be determined by calculating eigenvalues of these matrices. The natural frequencies are obtained by the following equation,

$$f = \left[\lambda/2\pi L_{fc}\right]\sqrt{E/\rho(1 - \mu^2)} \tag{56}$$

Where,

$$L_{fc} = R_f \times \theta + b_f$$

Mode shapes can be obtained by back substituting the values of λ in equation (49-52) and calculating eigen vectors.

3.2   Results and Discussion

Analytical results from the transfer matrix method are corroborated with finite element results.

3.2.1 Curved Plates

Curved plate dimensions: Radius (R_{cp}) = 0.054 m

Length (L_{cp}) = 0.054 m

Thickness (h_{cp}) = 0.0005 m

Material properties: Young's modulus (E) = 210 GPa

Poisson's ratio (μ) = 0.29

Density (ρ) = 7850 Kg/m^3

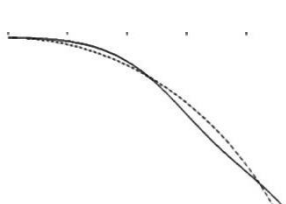Table 16: First six natural frequencies for C-C circumferential boundary conditions

Sr. No.	Transfer Matrix Method(Hz)	Finite Element Method (Hz)	% Error
1	5593.77	5585.10	0.15
2	5938.85	5934.40	0.07
3	8549.55	8537.30	0.14
4	9069.42	9050.80	0.20
5	9591.16	9570.90	0.21
6	11819.20	11770.00	0.41

Table 17: First six natural frequencies for S-S circumferential boundary conditions

Sr. No.	Transfer Matrix Method(Hz)	Finite Element Method (Hz)	% Error
1	3624.77	3680.40	-1.51
2	4399.24	4515.00	-2.56
3	7121.39	7099.50	0.30
4	7130.70	7203.90	-1.01
5	7395.85	7516.20	-1.60
6	8237.20	8261.00	-0.28

Table 18: First six natural frequencies for F-F circumferential boundary conditions

Sr. No.	Transfer Matrix Method(Hz)	Finite Element Method (Hz)	% Error
1	1496.06	1458.50	2.57
2	1496.06	1497.00	-0.06
3	3481.61	3484.10	-0.07
4	3586.66	3584.50	0.06
5	3610.40	3611.70	-0.03
6	5020.84	5024.90	-0.08

Table 19: First six natural frequencies for C-F circumferential boundary conditions

Sr. No.	Transfer Matrix Method(Hz)	Finite Element Method (Hz)	% Error
1	1505.51	1505.70	-0.01
2	3545.90	3547.80	-0.05
3	3956.87	3956.20	0.01
4	5649.72	5642.10	0.13
5	6180.34	6186.10	-0.09
6	7585.47	7579.00	0.08

Table 20: First six natural frequencies for S-F circumferential boundary conditions
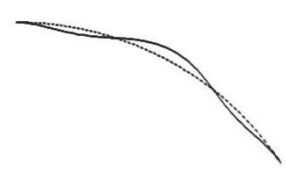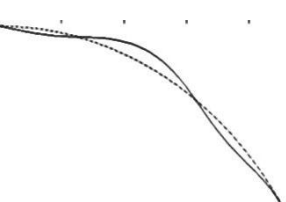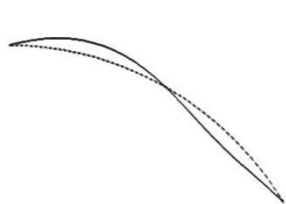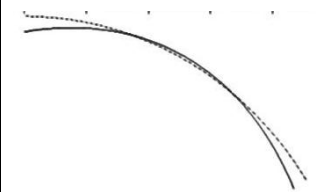
Sr. No.	Transfer Matrix Method(Hz)	Finite Element Method(Hz)	% Error
1	1491.55	1490.40	0.08
2	3460.03	3536.80	-2.17
3	3544.06	3546.20	-0.06
4	5004.00	5124.30	-2.34
5	6159.87	6139.70	0.32
6	6180.11	6185.90	-0.09

Table 21: First six natural frequencies for C-S circumferential boundary conditions

Sr. No.	Transfer Matrix Method(Hz)	Finite Element Method(Hz)	% Error
1	4104.57	4103.20	0.03
2	5290.28	5285.50	0.09
3	7469.98	7463.10	0.09
4	7786.20	7769.90	0.21
5	8791.23	8776.60	0.17
6	10213.7	10192.00	0.21

Table 16-21 shows first six natural frequencies of curved plate for different circumferential boundary conditions. It shows the comparison of TM method and FEM method. The last column of tables indicates the percentage of error between these two methods. Analytical results are in good agreement with FEM results. Table 22 shows the six mode shapes from FEM and transfer matrix method. First column of table characterizes the mode, the second column indicates the boundary conditions used and the third column gives the natural frequency of that mode.

Table 22: Mode shapes from Analytical and FEM methods for curved plate

Mode m,n	Circumferential boundary condition	TM Frequency (Hz)	TM mode shape	FEM mode shape
1,1	C-C	5593.77		
1,2	C-S	5290.28		
1,2	C-F	3956.87		
1,1	S-S	3624.77		

1,2	S-F	3460.03		
1,1	F-F	1496.06		

3.2.2 Cylindrical Duct

Cylindrical duct dimensions: Radius (R_{cd}) = 0.252m

Length (L_{cd}) = 0.732m

Thickness (h_{cd}) = 0.003m

Material properties: Young's modulus (E) = 207 GPa

Poisson's ratio (μ) = 0.3

Density (ρ) = 7830 Kg/m³

Table 23: Comparison of six natural frequencies of a cylindrical duct with FEM

Sr. No.	Transfer Matrix Method (Hz)	Finite Element Method (Hz)	% Error	Basem and Logesh [15]
1	282.32	284.43	0.74	269.00
2	323.35	331.09	2.33	315.00
3	366.50	365.66	-0.22	327.10
4	432.32	431.64	-0.15	420.80
5	578.81	571.47	-1.28	----
6	589.03	586.72	-0.39	573.00

Table 23 shows the results comparison of first six natural frequencies between transfer matrix method, finite element method and the results given by Basem and Logesh [15]. The percentage of error between transfer matrix method and FEM method is shown in the third column of the table. The maximum percentage of error is 2.33% which is quite acceptable. Basen and Logesh [15] conducted an experimental modal analysis of simply supported circular cylindrical ducts and results are given in the last column of the table. Analytical results are in good agreement with experimental results.

Table 24: Mode shapes of cylindrical duct from analytical method, FEM method and from reference paper.
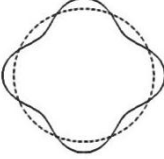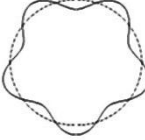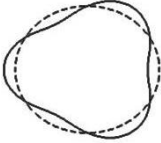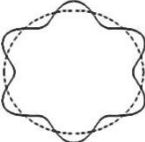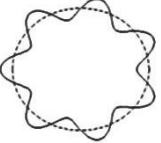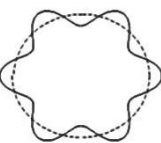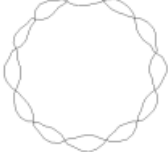
Mode m,n	TM Frequency (Hz)	TM mode shape	FEM mode shape	Basem and Logesh [15] mode shapes
1,4	282.32			
1,5	323.35			
1,3	366.50			
1,6	432.32			
1,7	578.81			--
2,6	589.03			

Table 24 shows mode shapes of cylindrical duct for first six modes. First column helps to characterize the mode shape.

3.2.3   Flat Oval Duct

Flat oval duct dimensions: Radius (R_f) = 0.038m

Width (b_f) = 0.06m (refer Fig.11 for more details)

Length (L_f) = 0.61m

Thickness (h_f) = 0.0006m

Material properties: Young's modulus (E) = 210 GPa

Poisson's ratio (μ) = 0.3
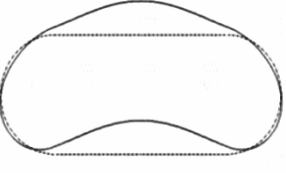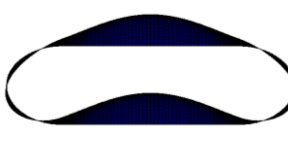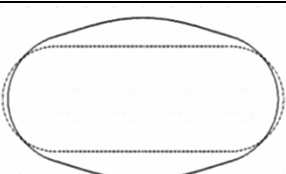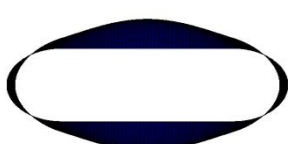
Density (ρ) = 7800 Kg/m^3

Table 25: Comparison of six natural frequencies of a flat oval duct with FEM

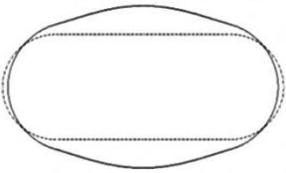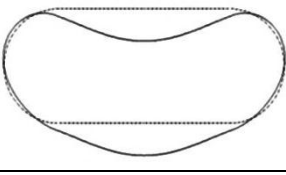| Sr. No.	Transfer Matrix Method (Hz)	Finite Element Method (Hz)	% Error
1	97.61	97.69	0.08
2	115.30	115.35	0.04
3	133.61	133.66	0.04
4	142.56	142.77	0.14
5	161.96	162.10	0.08
6	164.18	164.26	0.05

Table 25 shows a comparison of first six natural frequencies for the duct dimensions given above by using the transfer matrix method and finite element method. The last column of the table shows the percentage error in frequency calculation between two methods. The maximum percentage error is 0.14% between two methods. Error column clearly shows the validation and the accuracy of this method.

Table 26: First four mode shapes for flat oval duct

Mode m,n	TM Frequency (Hz)	TM mode shape	FEM mode shape
1,1	97.61		
1,1	115.30		
2,1	133.61		
2,1	142.56		

Only two types of symmetry-symmetry and symmetry-anti-symmetric modes are prominently seen for the first six natural frequencies of elliptical ducts with increasing half wave numbers in axial direction. Table 26 shows the first four mode shapes of flat oval duct. First and fourth are symmetric mode and second and third are antisymmetric modes with increasing half wave numbers in axial direction.
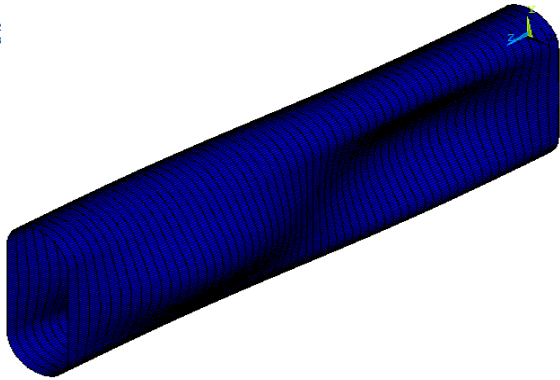
Figure 1(a): Third mode shape with m=2   **Figure 12 (b): Fifth mode shape with m=3**
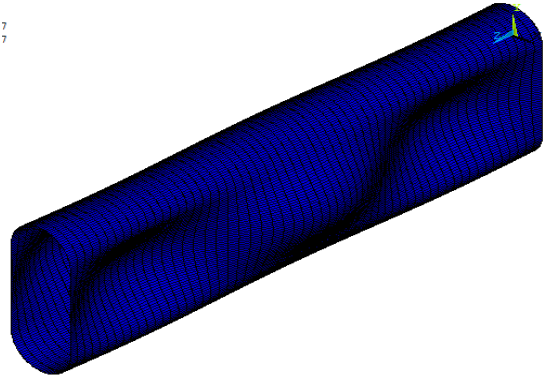
Figure 12 (a) shows third mode shape with half axial wave number m=2 and 12 (b) shows fifth mode shape of a flat oval duct with half axial wave number m=3.

Chapter 4

Experimental Modal Analysis

In this chapter, measurement of modal parameters has been discussed. Experimental Modal Analysis (EMA) has been done for a beam and elliptical duct. This chapter explains about the setup for EMA with different boundary conditions, result analysis. Discussed about a procedure to correlate EMA results with FEM results using Modal Assurance Criteria (MAC).

4.1   Cantilever Beam

Simplest structure for analyzing EMA is a beam with clamped at one end. This structure modeled as cantilever beam.

4.1.1   Instrumentation and Experimental Setup

Figure 13 shows the experimental setup for a cantilever beam. 'C clamp' is used to give clamped condition at one end, this may not be an exact clamped condition but it approximate clamped conditions. Assuming plate has homogeneous material properties and uniform thickness along the length.

Figure 13: Experimental setup for cantilever beam

Dimensions of cantilever beam are 39cm length, 3cm width and 0.33cm thickness.

A high sensitivity, uniaxial, a light weight accelerometer is used to pick up vibration response. Sensitivity values are provided by manufacture itself. Accelerometer mounting position is an important and is decided by prior FEM analysis. As the maximum deflection is at the end of the plate of a cantilever beam, an accelerometer is mounted at the end of the plate (as shown in Fig.13). Mounting methods of these accelerometers are important because they affect usable frequency range. There are different mounting conditions are possible like stud mounting, wax mounting, holding by hand. In this analysis wax mounting is used for mounting the accelerometer to beam because it is an easy and fast way of mounting. Care has to be taken on thickness of wax mounting used because it affects readings as stiffness changes.

Impact hammer is used for inducing vibrations in the structure. Impact hammer mainly consists of two parts, tip of the hammer and a force transducer connected to the tip. Tip of the hammer is decided based on the frequency range of interest which is decided by FEM analysis. A major factor which controls the frequency range of interest is hardness of hammer tip and compliance of impact surface. Minor factors are weight of the hammer and impact velocity. One more critical factor which controls the tip and weight of hammer is double impact. Double impact should be avoided while taking measurements as it increases noise in the measurements. The light weight hammer is useful for avoiding double impact. As in this cantilever beam case our frequency range of interest is low and chances of getting the double impact problem are more so, hammer chosen for analysis is with harder tip, light weight. High impact velocity is also useful to avoid double impact.

Experimental plate has been divided into 13 parts each part of 3 cm length i.e. total 14 grid points have been generated along plate length. The accelerometer is placed at the 14th point location which is the free end of the plate. Measurement has been done at all grid points by giving one by one impact at every grid point by using a hammer. Fixing the accelerometer at one location and moving the hammer for every measurement is called roving hammer technique.

"m + p international SO Analyzer Rev. 4.1" hardware and associated software is used for data acquisition and processing purpose. Force transducer from impact hammer is connected to first input channel which is excitation input for software and the accelerometer is connected as the second input. Then this time domain data is converted to frequency domain data using Fast Fourier Transform (FFT) in the software. Then software creates Frequency Response Function (FRF) between two inputs. As the roving hammer method is used for analysis, software treats the excitation signal as a response signal and transducer (accelerometer) signal as a reference signal to calculate FRF.

4.2   Elliptical Duct
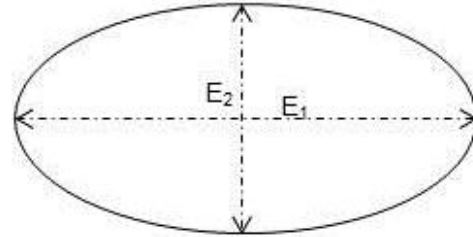
EMA of elliptical duct is more complex than a simple cantilever beam problem. Figure 14 (a) shows the elliptical duct geometry and its cross section. It is manufactured by using hand bending process. Lap joint is used to join two ends which is also created by hand and hammer. So the final shape of the ellipse is slightly distorted from the perfect ellipse and also lap joint increases the local

stiffness of the structure. Figure 14 (b) shows the elliptical duct cross-section model. It's a perfect elliptical shape.

| Figure 14 (a): Actual elliptical duct | Figure 14 (b): Modeled elliptical duct |

Experimental modal analysis of elliptical duct is done by using two approaches, Single Degree Freedom (SDOF) system approach and Multi Degree Freedom (MDOF) system approach.

4.2.1 Single Degree Freedom (SDOF) System

SDOF system estimates natural frequencies, mode shapes, damping using single degree freedom (SDOF) estimation algorithm. Modal frequencies are the roots of the characteristic equation of systems and contain information about damping and natural frequencies. SDOF analysis is used for systems having distinct roots i.e. different modal frequencies like cantilever beam. Even this approach is used for other systems also to get the basic information because it is simpler than MDOF approach. SDOF approach needs only one reference point i.e. only one accelerometer is enough. Two different algorithms are possible in this software for SDOF, Finite Difference and Quadrature algorithm. Finite difference gives the complex roots where Quadrature algorithm gives real roots. Ideally linear systems have real roots. So quadrature algorithm is used for analysis.

4.2.2 Multi Degree Freedom (MDOF) System

Most of the practical structure will have repeated roots or pseudo-repeated roots. This is more general in symmetric structures but can possible in unsymmetrical structures also. Repeated roots mean, one or more modes will have the same natural frequency. Pseudo-repeated roots means, modal density is very high so the modes are very closely spaced. Analytically these two are different things but practically they are one and same. With SDOF approach it won't be possible to get these repeated or pseudo-repeated roots as they're only one reference data is used. MDOF approach solves this problem with multi reference data. Maximum number of repeated or pseudo-repeated roots that can be calculated depends on the number of references used. Five different references are chosen in the current investigation.

4.2.3 Instrumentation and Experimental Setup

Figure 15 shows the experimental setup for elliptical duct with free – free boundary conditions. Experimental elliptical duct is hanged in air by using rubber tubes. As stiffness of these rubber tubes are very less as compared to duct, so this hanging material doesn't affect much on results of modal analysis. These conditions approximate free – free boundary conditions. External frame and the rod which is used to tie rubber tubes are of steel material which gave enough strength to withstand with impact force.

Figure 15 (a): General Set up for Elliptical Duct   **Figure 15 (b): set up for MDOF system analysis**

Accelerometer, impact hammer, software and hardware details are same as used for cantilever beam given in the previous subsection. Analysis is done in two methods, SDOF system and MDOF system. Figure 15 (b) shows the arrangement of accelerometers for MDOF system analysis. In MDOF system analysis, four accelerometers are used for measurement. Positions of these accelerometers are shown in Fig. 15 (b). Only one accelerometer is enough for SDOF system analysis which is placed at the 5th position (in MDOF fig. only accelerometer at 5th position for SDOF). These accelerometer positions have been decided based on prior FEM analysis of elliptical duct.

The experimental elliptical duct has been divided into 80 (16×5) grid points. Sixteen points along cross section and a total of 5 cross sections along the length. As the roving hammer method is used for analysis, hammer is used to excite structure at all 80 points and measurement has been taken at some points which was decided from FEM analysis.

4.3   Result and Discussion

After recording time domain data, software itself will convert that data into frequency domain data and results will be displayed in form of FRF. After getting all FRFs data need to be analyzed to get the correct information about modal parameters. All FRF contains the peak values and information about modal parameters but only driving point FRF is used for getting natural frequencies as this is

more reliable data than any other FRF data but for animating mode shape software considers all peaks from all FRF data. Driving point is the point where the accelerometer is placed and impact also given. That's why driving point reading is very important while recording the data. Though FRF shows peaks clearly it doesn't mean that it has to be related with mode of system because it can be operating deflection shape also. There are two ways to decide whether it is mode shape or operating deflection shape. One is an imaginary plot of FRF data, which shows peaks in one direction either on the positive side or negative side depends on impact direction and accelerometer orientation. All peaks of an imaginary plot of driving point FRF on same direction refers to the modes of the structure. Another method is to see the amplitude and phase plot. At the modal frequency there will be a 180 degree change in phase on phase plot.

It is also important to see coherence plots, which tells how output is varying with respect to input. Coherence values will be between 0 and 1. Especially at antinode location coherence values will be near 1 and node locations deeps in coherence values can be seen.
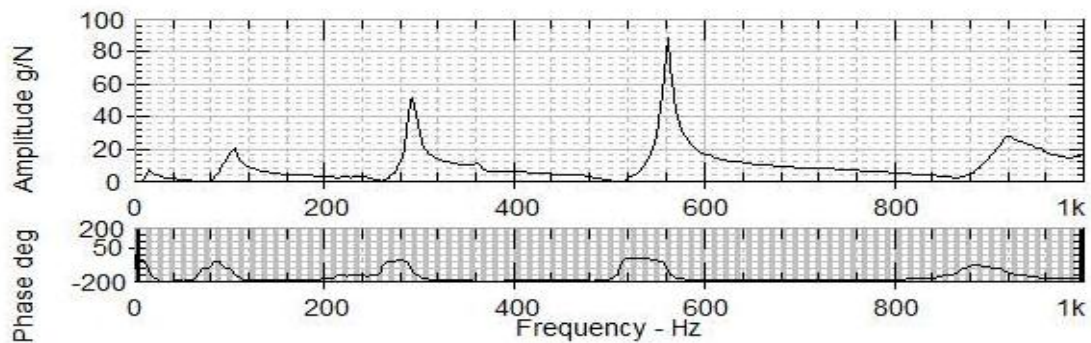
4.3.1 Cantilever Beam

Plate dimensions: 0.39 m length, 0.0033 m thick.

Figure 16 shows the imaginary part of FRF at driving point of the cantilever beam. Five different peaks can be clearly seen from Figure.
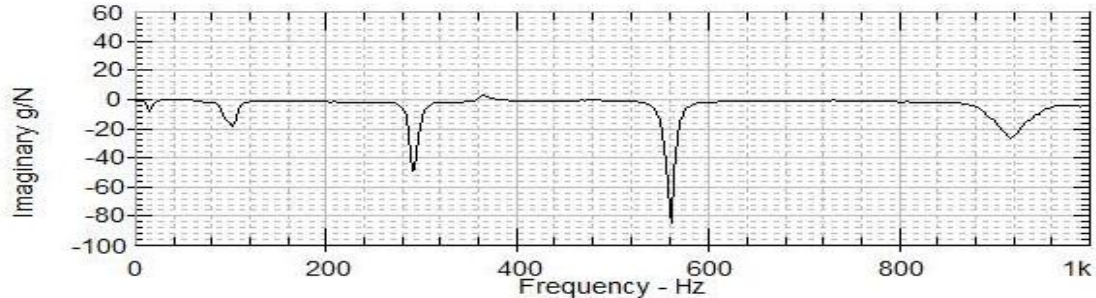

Figure 16: Imaginary component of driving point FRF

Figure 17: Amplitude & phase plot of driving point FRF

Figure 17 shows the amplitude and phase plot at driving point which can also be used to identify the natural frequencies. Figure 17 clearly shows the peaks and at the same peaks there is a 180 degree phase change can be seen in phase plot, which indicates that these are nothing but natural frequencies of the beam.
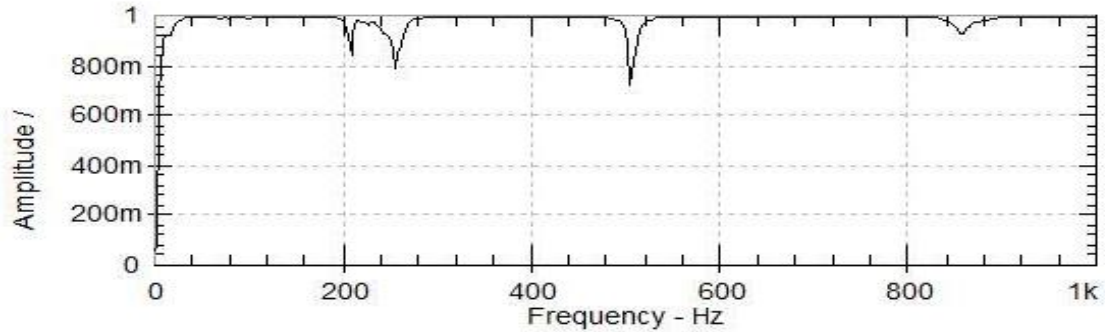
Figure 18: Coherence at driving point

Figure 18 shows coherence at driving point of the beam. Where ever peaks are there in the FRF at those locations coherence amplitude is almost 1 in coherence plot, which indicates that data is very reliable.

Table 27 shows the comparison of natural frequencies and mode shapes between EMA results and FEM results. Variation in data is mainly due to an assumption of uniform thickness in FEM analysis.

Table 27: Comparison of five natural frequencies and mode shapes of a cantilever beam with FEM

Sr. No.	Natural frequency (Hz)		Mode Shape	
	EMA	FEM	EMA	FEM
1	15.8	17.7		
2	101.4	111.2		
3	292.0	311.6		
4	561.5	611.8		
5	914.6	1013.9		

43

4.3.2   Elliptical Duct

Dimensions of elliptical duct are Major axis: 0.15 m,

Minor axis: 0.11 m,

Length: 0.61 m, and thickness: 0.0006 m

This duct is made up of steel material.

Figure 19 shows the imaginary part of FRF at driving point of elliptical duct. Distinct peaks on one side of the axis can be clearly seen in the Figure 19. Which represents the natural frequencies of elliptical duct.
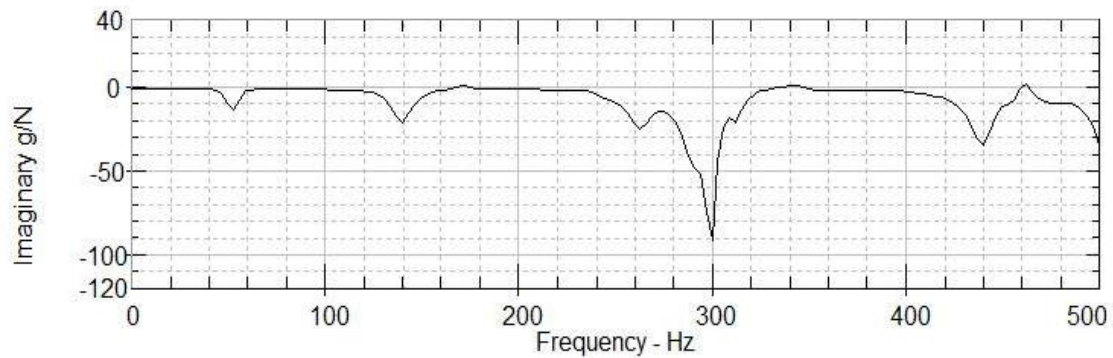

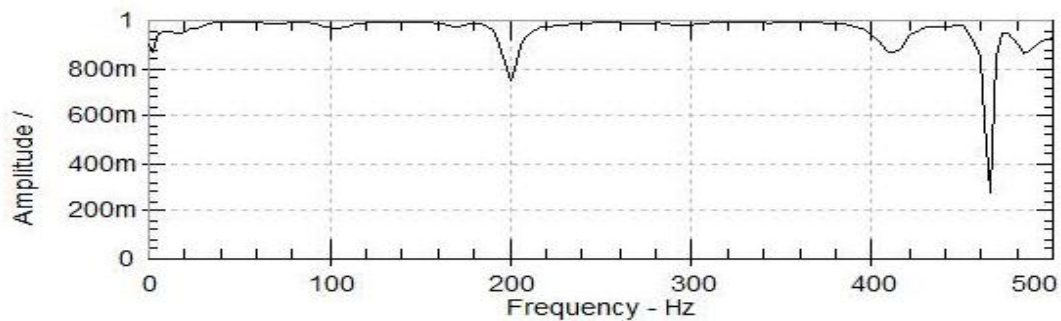
Figure 19: Imaginary component of driving point FRF

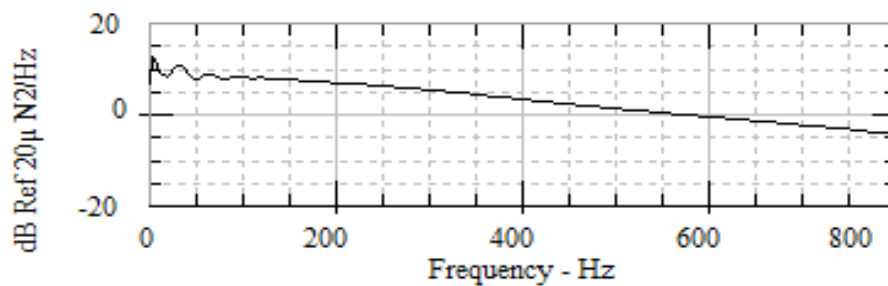**Figure 20: Coherence at driving point**

Figure 21: Average PSD graph for elliptical duct

Figure 20 and 21 shows the coherence at driving point and average PSD (Power Spectral Density). PSD graphs are useful to decide up to how much frequency range data are useful. Mainly up to 5-10 dB reduction in the input force spectrum in interest frequency range is acceptable. In the average PSD graph, there is 10 dB drop-off in input force can be seen, so the useful frequency is restricted up to 600 Hz only.

Table 28: Comparison of five natural frequencies of elliptical duct (as SDOF) with FEM

Sr. No.	Experimental Modal Analysis	Finite Element Method
1	53.13	64.77
2	140.63	180.19
3	300.00	342.31
4	440.63	561.63
5	525.00	610.82

Table 28 shows the comparison between first five natural frequencies from SDOF analysis and respective FEM analysis. FEM results shown that there is a need of MDOF analysis as the system has repeated roots which can't be seen in SDOF analysis.

MDOF results:

After capturing responses, data is analysed by using the advanced MDOF tool. Figure 22 shows the frequency range selection and mode indicator diagram with multivariate indicator function.
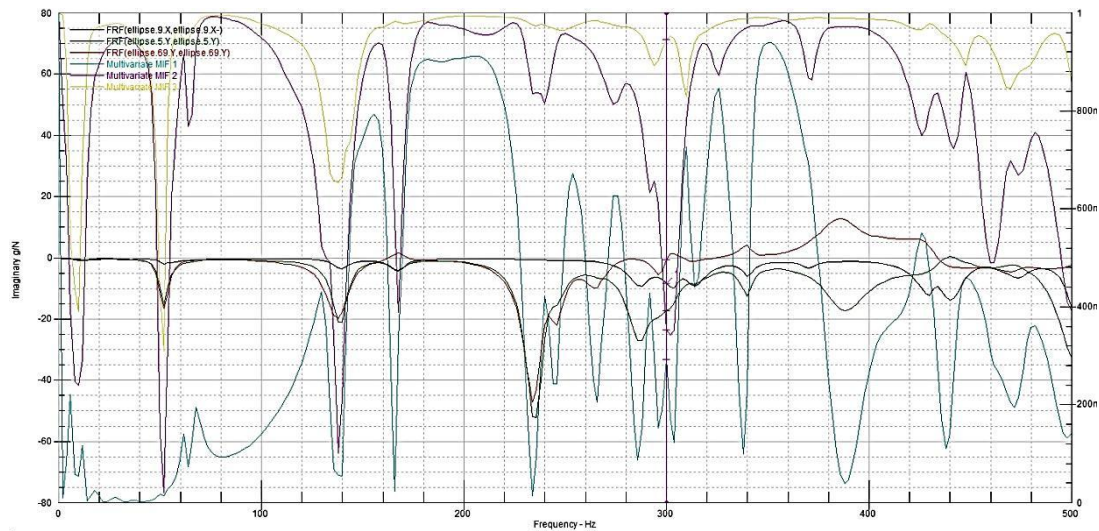
Figure 22: Frequency range selection and mode indicator diagram.

Multivariate (MvMIF) indicator function is selected to analyse the modes. MvMIF is the real valued frequency domain function with local dips at the natural frequencies of the system. For each reference data software will generate one MvMIF curve. Primary MvMIF curve dips at each of the natural frequencies. The secondary MvMIF curve dips at each natural frequency with repeated or

pseudo-repeated roots of order two or more. The additional MvMIF curves dips at each natural frequency with repeated or psudo-repeated roots of successively higher order. By counting the number of curves that dips at an interest frequency, one can estimate the number of modes at that frequency.
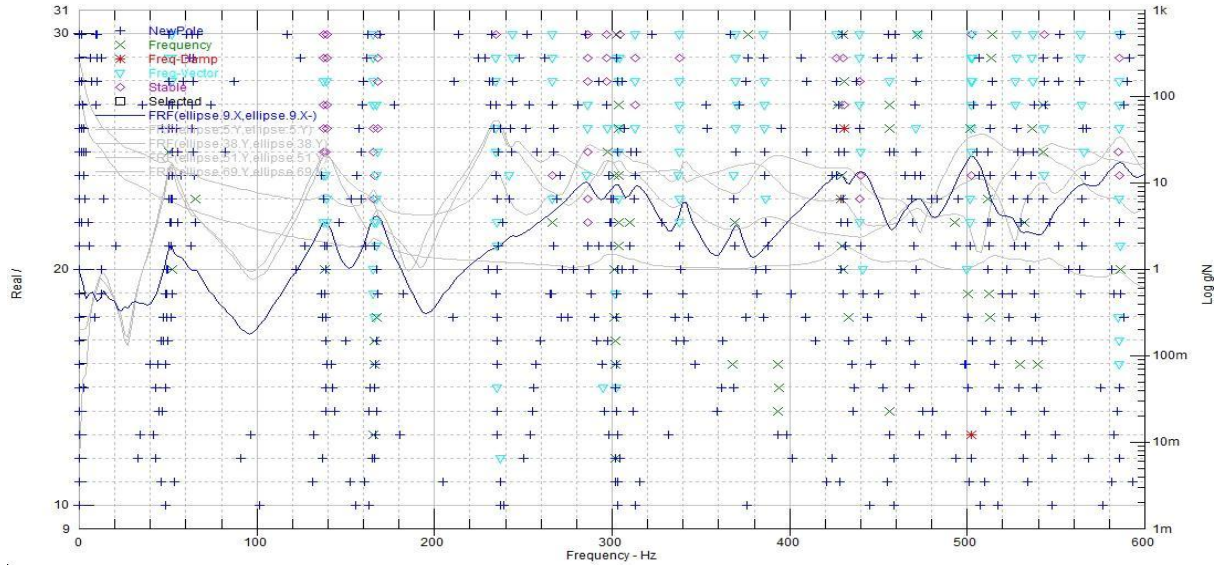
Figure 23: Stability diagram of MDOF analysis

Figure 23 shows the stability diagram for MDOF analysis of elliptical duct. This diagram used to select the poles at interest frequency as it shows the poles with stability levels. Stability levels are differentiated by different symbols and colors. Maximum stability indicated by ◇ (stable).

4.4 Correlation Analysis

Correlation analysis is used for the modal verification between experimental modal analysis data and FEM data. A modal assurance criterion (MAC) is used to define the correlation between these two models. MAC compares two modal vectors, EMA vector and FEM vector. In this comparison MAC matrix is generated. Values of the MAC will be between 0 and 1. If vectors are orthogonal to each other MAC value will be zero and if they are same it will be one. Normally a MAC value above 0.7 is considered as acceptable.

If V_i^{EMA} is modal vector from EMA and V_j^{FEM} is from FEM, then MAC is given as,

$$MAC_{ij} = \frac{\left|\{V_i^{EMA}\}\{V_j^{FEM}\}\right|^2}{\left\{\{V_i^{EMA}\}\{V_i^{EMA}\}\right\}\left\{\{V_j^{FEM}\}\{V_j^{FEM}\}\right\}} \tag{57}$$

For this analysis, experimental data is used as reference data because it represents actual conditions and FEM data is used as verification data.

4.4.1 MAC calculation for Beam

Correlation results are given in the form of modal pair comparison graphs and modal pair table. Figure 24 shows the correlation modal pair graph. Red colour indicates the values greater than 0.9 and green colour shows values less than 0.2. The graph shows the closeness between the respective modes of FEM data and EMA data.
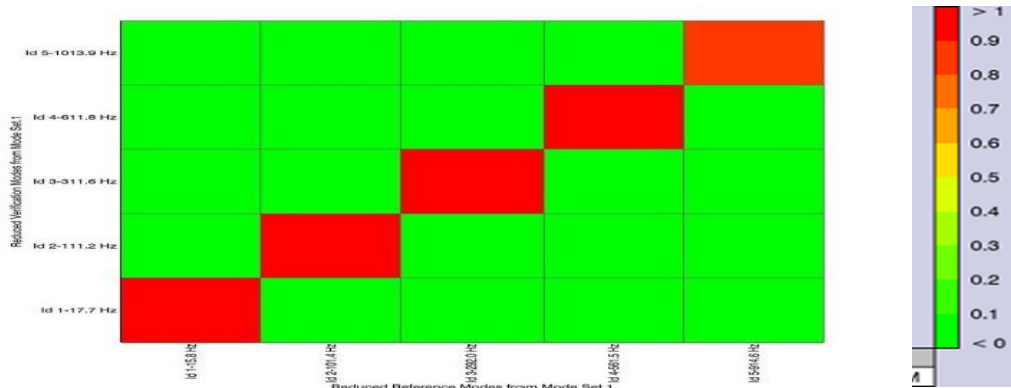
Figure 24: Modal assurance criteria - Matrix graph

The exact values of a MAC number between respective frequencies are given in the Table 29.

Table 29: MAC pair table between EMA and FEM data for cantilever beam

EMA	FEM	MAC Value
15.8	17.7	0.99
101.4	111.2	0.96
292.0	311.6	0.98
561.5	611.8	0.95
914.6	1013.9	0.90

4.4.2 Elliptical Duct

Figure 25 shows matrix graph of MAC number for an elliptical duct. EMA results generated on distorted elliptical duct and FEM conducted on perfect elliptical shape.
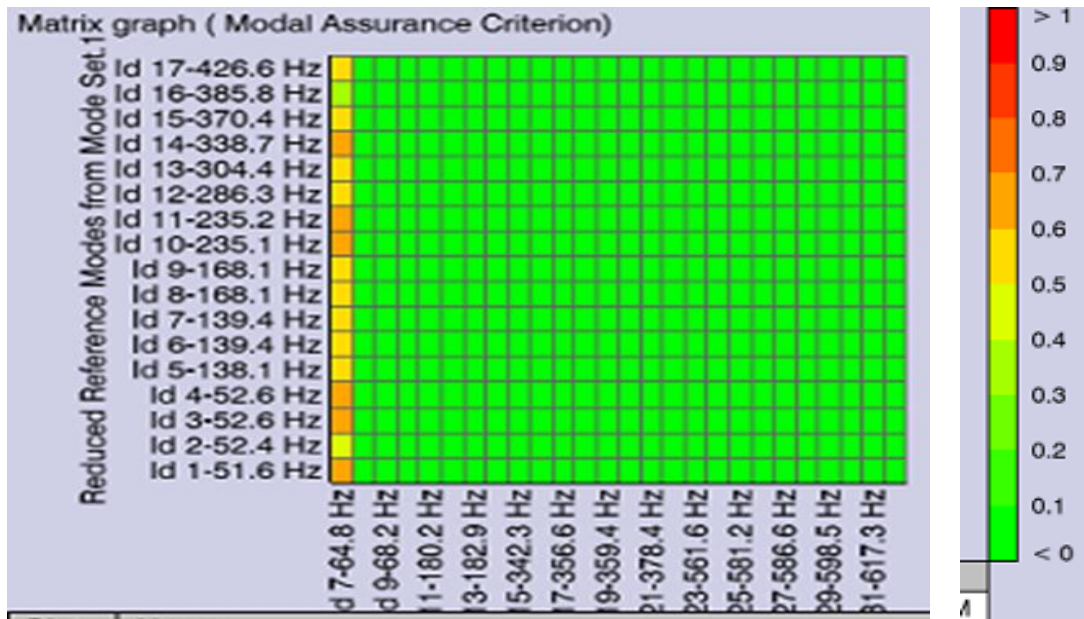
Figure 25: Modal assurance criteria – Matrix graph for elliptical duct

Matrix graph shows that the only first mode is matching with FEM data all others have fairly low values of MAC number. Table 30 shows the values of a MAC number between EMA and FEM frequencies.

Table 30: MAC pair table between EMA and FEM data for elliptical duct

FEM	EMA	MAC Value
64.8	51.6	0.621
75.9	138.1	0.019
182.7	168.1	0.004
342.3	304.4	0.003

It is evident from the MAC pair table and matrix graph that with distorted elliptical shape and with manufacturing limitations, it is possible to predict only first mode shape correctly. Considering shape distortions and also properties in Analytical modeling is necessary.

Chapter 5

Finite Element Analysis (FEM) Details

In the present chapter, Finite Element Analysis (FEM) is mostly used for validation purpose of analytical models. In an experimental modal analysis before setting up the actual analysis, modal characteristics of the elliptical ducts were examined by using FEM. This helps in deciding the frequency range of interest, accelerometer positions, impact hammer conditions, measurement points etc.

5.1   Software and Meshing Details

ANSYS 13 software is used for the finite element analysis purpose. Block Lanczos scheme used for modal analysis. Shell 63 elements are used. Details of no. of elements used are as given below,

Meshing Details:

1. For Rectangular Duct:

    1800 total elements, 60 along cross-section and 30 along length of duct.

2. For Curved Plate:

    1800 total elements, 60 along circumference side and 30 along length of plate.

3. For Cylindrical duct:

    1500 total elements, 60 along circumference and 25 along length of duct.

4. For Flat oval duct:

    720 total elements, 48 along circumference and 15 along length of duct

5. Cantilever Beam:

    405 total elements, 9 along cross-section and 45 along length of duct

6. For Elliptical Duct:

    3200 total elements, 80 along circumferential and 40 along length of duct

5.2   Boundary Condition Details

1.   For Simple support: The deflection perpendicular to the supports and rotation perpendicular to the plane is restricted.

Example: on X-Y plane: Z- direction rotation is constrained.

X- axis line deflection in Y- axis direction is restricted, and on the Y- axis line defection in X- axis are restricted.
One more additional restriction is given i.e. deflection in the Z-direction in order to stop rigid body modes.

Or

Simplified way to give simply supported boundary conditions is, if cross section is in X-Y plane constrains the deflections in these both directions.
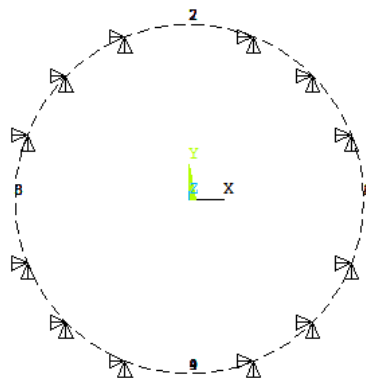
Figure 26: Front view of cylindrical duct with simply supported boundary condition

2.   For Clamped support: All degrees of freedom restricted for the respective lines.

\Chapter 6

Conclusions

Simple and accurate analytical methods have been explored for free vibration analysis of rectangular, cylindrical and flat oval duct. Mainly transfer matrix method is used for analysis of these ducts which is capable of considering simply supported axial boundary conditions. Rayleigh – Ritz method is used for analysis of rectangular ducts with different axial boundary conditions. The results of these methods show a good amount of accuracy (more than 95%) in comparison with FEM results and available literature results. This validated analytical model is used to generate tabular data consisting of non-dimensional frequency parameters for different side and aspect ratios of rectangular ducts. This is done by using extensive parametric study on different dimensions of rectangular ducts. This data can be useful as direct engineering solutions for free vibration problems of different dimensions (specified in the table) of rectangular ducts. One more advantage of this data is different material properties can be incorporated while calculating natural frequencies by using this data. Curve fitting has been done for this data to arrive at simple empirical relation. This empirical relation can be used to calculate the first fundamental frequency for any combination of aspect ratio and side ratio between range (0.25 to 1) with prediction error less than 5%. Rectangular mode shapes are classified into four groups and notation is introduced for easy understanding of typical vibration characteristics.

Flat oval duct results are compared with FEM data for validation of method. There are no literature data available for this duct geometry. Predominantly two types of mode shapes i.e. symmetry-symmetry and symmetry-antisymmetry shapes can be seen at lower modes. Experimental Modal analysis is illustrated for free vibration analysis of cantilever beam and elliptical duct. Elliptical ducts are analyzed by using two methods (SDOF and MDOF) as there are repeated roots for the structure. Results of both are compared with FEM results. Validation of mode shapes is done by using correlation analysis between EMA and FEM data. MAC number values for respective modes of cantilever beam are in good agreement (above 0.9). For elliptical ducts correlation analysis is able to match first mode. It concludes that distorted shape and joint conditions play an important role in estimating mode shapes. Only first modes can be correctly predicted by using numerical analysis, with ideal cross-section dimensions.

The transfer matrix method needs to be explored for different axial boundary conditions. Numerical analysis needs to improve to accommodate manufacturing errors and joint conditions for elliptical duct. Experimental Modal Analysis needs to be done with perfect elliptical duct with different boundary conditions to validate the results with numerical and analytical results. The acoustical characteristics of these ducts need to be explored as the second step towards understanding of coupling phenomenon.

Chapter 7

Appendix

Elements of state space matrix of equation 1 are as follows,

$A_{12} = -(m\pi/l)$

$A_{21} = \mu(m\pi/l)$

$A_{43} = -\mu(m\pi/l)^2$

$A_{45} = 1/h$

$A_{63} = -(1 - \mu^2)h(m\pi/l)^4 + (12/h)\lambda^2$

$A_{81} = -12(1 - \mu^2)(1/h)(m\pi/l)^2 + (12/h)\lambda^2$

$A_{18} = -h/6(1 - \mu)$

$A_{27} = h/12$

$A_{34} = -1$

$A_{54} = 2(1 - \mu)h(m\pi/l)^2$

$A_{72} = -(12/h)\lambda^2$

References

[1] B. Venkatesham, Mayank Tiwari and M. L. Munjal 2011, *International Journal of Acoustics and Vibration*, Vol. 16, "Prediction of breakout noise from a rectangular duct with compliant walls".

[2] B. Venkatesham, Mayank Tiwari and M. L. Munjal 2010, *Noise Control Engg. J.* 58(3), "Prediction of breakout noise from an elliptical duct of finite length".

[3] S. Azimi, W. Soedel and J.F. Hamilton 1986, *Journal of Sound and Vibration* 109(1), 79-88, "Natural frequencies and modes of cylindrical polynomial ducts using receptance method".

[4] G. Yamada, K. Kobayashi 1987, *Journal of Sound and Vibration* 115, 363-364, Comments on "Natural frequencies and modes of cylindrical polygonal ducts using receptance methods".

[5] H. P. Lee 1993, *Journal of sound and Vibration* 164, 182-187, "Natural frequencies and modes of cylindrical polygonal ducts".

[6] T. Irea, G. Yamada and H.Ida 1985, *Journal of Sound and Vibration* 102(2), 229-241, "Free vibration of longitudinally stiffened prismatic shells with and without partitions".

[7] S. J. Mohan, R. Pratap 2004, *Journal of Sound and Vibration* 269, 745-764, "A natural classification of vibration modes of polygonal ducts based on group theoretical analysis".

[8] T. Irie, G. Yamada and K. Tanaka 1984, *Journal of Sound and Vibration* 95(1), 131-135, "Natural frequencies of folded plates".

[9] T. Irie, G. Yamada and Y. Kobayashi 1984, *Journal of Sound and Vibration* 96(1), 133-242, "Free vibration of non-circular cylindrical shells with longitudinal interior partitions".

[10] T. Irie, G. Yamada and Y. Muramoto1984, *Journal of Sound and Vibration* 95(1), 31-39, "Free vibration of joined conical – cylindrical shells".

[11] T. Irie, G. Yamada and Y. Kaneko 1982, *Journal of Sound and Vibration* 82(1), 83-94, "Free vibration of a conical shell with variable thickness".

[12] Zhou Ding 1996, *Journal of Sound and Vibration* 189(1), 81-87, "Natural frequencies of rectangular plates using a set of static beam functions in Rayleigh-Ritz method".

[13] Zhou Ding and Y. K. Cheung 1996, *Journal of Sound and Vibration* 223(2), 231-245, "Free vibration of line supported rectangular plates using a set of static beam functions".

[14] Tian Ran Lin and Jie Pan 2009, *Journal of Vibration and acoustics* 131, "Vibration characteristics of box type structure".

[15] Basem Alzahabi and Logesh Kumar Natrajan, "Correlation of Modal Analysis of Circular Cylindrical Shells".

[16] Guanmo Xie 2011, *International conference, Electric Information and Control Engineering*, "Free vibration of circular cylindrical shells using transfer matrix method"

[17] M. Ohga, H. Takag and T. Shigfmatsu 1995, *Journal of Sound and Vibration* 183(1), 143-156, "Natural frequencies and mode shapes of open cylindrical shells with a circumferential thickness taper".

[18] ANSYS 13, *User Manual*, ANSYS Inc.

[19] m + p international SO Analyser Rev. 4.1, *User Manual*.

[20] LMS Virtual Lab REV 10 -SL2, *User Manual*.